



**5G Communication with a Heterogeneous, Agile Mobile network in the Pyeongchang Winter Olympic competition**

Grant agreement n. 723247

# Deliverable D5.2
# 5G Satellite Communication analysis - final version

| | |
|---|---|
| **Date of Delivery:** | 1 June 2018 |
| **Editor:** | Thibault Deleu |
| **Associate Editors:** | Mathieu Gineste |
| **Authors:** | Nicolas Chuberre, Michel Cohen, Thibault Deleu, Raffaele D'Errico , Jean-Baptiste Doré, Mathieu Gineste, Markus Mueck, Visvesh Saravanan |
| **Dissemination Level:** | PU |
| **Security:** | Public |
| **Status:** | Final |
| **Version:** | V1.0 |
| **File Name:** | 5GChampion_D5.2_Final |
| **Work Package:** | WP5 |

| Modifications | Date | Version |
|---|---|---|
| Initial document | | |
| | | |


## Abstract

This document investigates seamless operation of UE in the 5G architecture via a satellite or a HAPS component, targeting narrowband IoT and voice services. The study shows that 5G UE can operate at low bitrate through satellite components with minimum configuration update providing a continuity of service and complementing terrestrial infrastructure for narrowband IoT services. With current technologies the capacity that could be provided through satellite or HAPS components permits to reach high density of user served per square kilometer significantly increasing the number of served objects.



## Index terms

Narrowband IoT, Satellite Communication, 5G networks, seamless integration

## Contents

# Table of Figures

# 1 Introduction

Today an estimated 15 billion of connected objects communicate with each other's. These connected objects that compose the Internet of Things (IoT) are expected to extend to 50 or 80 billion worldwide by 2020. Bringing wide-area connectivity for the IoT using satellite technology is therefore an attractive solution to complement terrestrial networks, allowing densification and coverage extension in remote areas.

This document analyses and defines the 5G interoperability architectural framework and technical enablers allowing operation of 5G UE via a satellite communication component, assess the performance of 5G radio interface via different space component type (GSO, NGSO). It describes the necessary modifications to operate on 5G systems in order to take satellite and HAPS specifics into account.

Firstly, it reviews state-of-the art waveforms designed for IoT communications. The waveforms are compared in terms of amplitude variation and capacity. A new waveform, turbo-FSK is proposed to enhance performance of existing waveforms.

Based on the proposed waveforms, link budget calculations and system dimensioning, including channel modelling, are provided to determine the required satellite and HAPS performance as well as to estimate the number of served users per km².

This document finally specifies a test bed to demonstrate the 5G interface performance via selected space segment configurations under representative interference/mobility conditions.

# 2 5G Mobile/Satellite Convergence

## 2.1 Concept

Enabling standard user equipment to access 5G via satellite in addition to cellular network, as shown in Figure 2-1, will open new market and usage opportunities. In this study, low data rate services are targeted such as:

- Users of the consumer market, which may travel to areas without or simply out of order cellular network infrastructure

- Machine Type Communications and personal emergency communications that can address critical applications especially in the area of security, transportation, automotive and energy/water utilities sectors

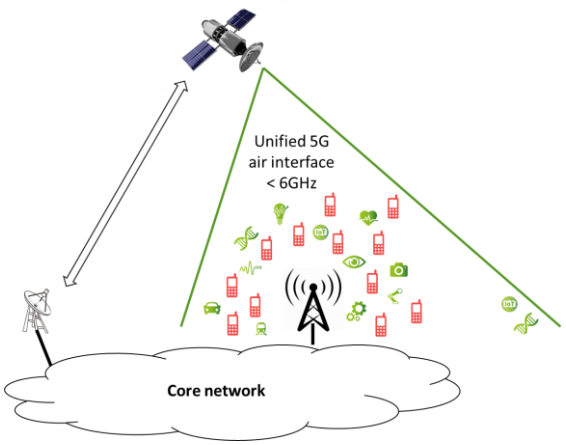


***Figure 2-1: Satellite MTC unified air interface concept***

## 2.2 Reference architecture

Figure 2-2 gives the reference architecture of the hybrid satellite-terrestrial access network, requiring a smart resource management. The user terminal has seamless ubiquitous access to satellite and terrestrial links for low data rate services. The satellite eNodeB (which is located on ground in case of non-regenerative satellites) exhibits enhanced MAC capabilities (soft interference cancellation techniques, interference management…).

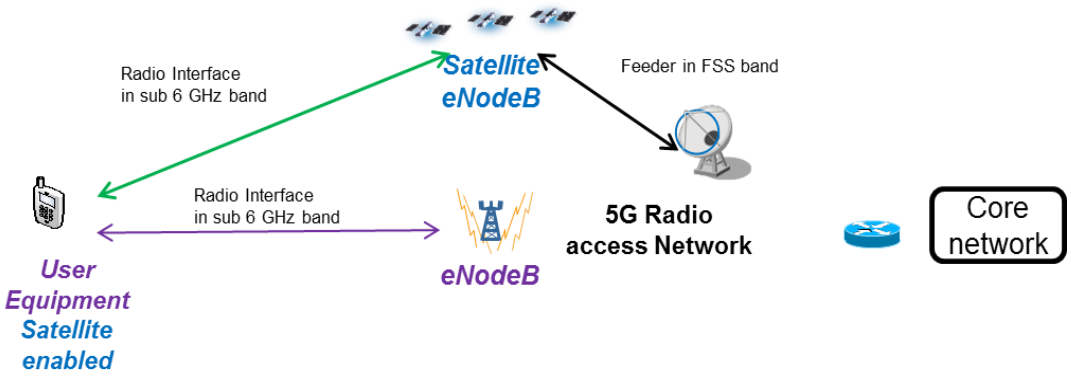


***Figure 2-2: Architecture for hybrid satellite-terrestrial access network in a 5G scenario (regenerative satellite)***

### 2.2.1 Frequency bands

It is assumed that the system operates in S-band with a 30MHz system bandwidth:

- Uplink (User to Satellite) : 1980-2010 Mhz
- Downlink (Satellite to user): 2170-2200 MHz

The link between the satellite eNodeB and the feeder is in the FSS band.

### 2.2.2 Terminal

The terminal will operate in S band.

For the link budget calculations, we assume a Class 3 terminal with the following characteristics

- Antenna gain : 0 dBi
- Polarization: linear
- Noise Figure :
    - 9 dB Baseline
    - 6 dB as a credible alternative
- EIRP : 23 dBm ➔ -7 dBW
- G/T (figure of merit): two possible values
    - -33.6 dB/K with Noise Figure of 9 dB
    - -30,6 dB/K with Noise Figure of 6 dB.

Note : the standard terminal has an antenna of linear polarization, while satellite antennae are of circular polarization. The consequence is a polarization mismatch of 3 dB leading to following values

- Equivalent EIRP of 20 dBm (-10 dBW) under satellite coverage.
- Equivalent G/T of -36,6 dB/K or -33,6 dB/K

### 2.2.3 Space segment

#### 2.2.3.1 Satellite orbits

To provide mobile satellites services satellites at different altitudes can be considered:

- Geostationary satellites : 1 to 3 satellites at 35786 km altitude are needed in order to cover the world between 70 ° Latitude North and 70 ° Latitude South
- Medium Earth Orbits (MEO) satellites between 6000 and 10000 km altitude and around 10 to 12 satellites to insure a worldwide coverage. Two orbits can be considered:
  - Inclined orbits at 45 ° with 2 inclination plans
  - Polar orbits with 2 or 3 inclination plans
- Low Earth Orbit (LEO) satellites between 800 and 2000 km altitude and 50 to 100 satellites to insure continuous coverage with multiple visibility part 100 % of the time in a given point on earth. Again, two orbits are considered:
  - Inclined orbits at around 52°
  - Polar orbits or near polar orbits at 89°inclination
  -

For the different link budgets computations, we will consider the following systems

- GEO satellite at 36000km
- MEO constellation at 10000 km
- LEO constellation at 1500 km
- LEO constellation at 800 km

#### 2.2.3.2 Space segment architectures

Different architectures can be considered for the space segment and are summarized in Table 2-1. For transparent satellites, the gateway always involves the virtualized evolved packet core (vEPC) interface, the radio network controller (RNC) and the eNodeB. For regenerative satellites, the satellite always involves the eNodeB while the gateway always involves the vEPC interface. The RNC can be either located in the satellite or in the gateway.

***Table 2-1: Possible space segment architecture***

| **Satellites** | **Gateway** |
|---|---|
| **Transparent** | vEPC interface + RNC + eNodeB |
| **OBP option 1 (eNodeB)** | vEPC interface + RNC |
| **OBP option 2 (RNC + eNodeB)** | vEPC interface |

#### 2.2.3.3 Satellite impairments

Different impairments are produced on communication signals by the satellite:

- Doppler shift due to satellite motion, especially for non-GEO satellites. Maximum Doppler shift are given in Table 2-2, considering a 2GHz signal. The maximum Doppler rate is around 170Hz/s.

***Table 2-2: Maximum Doppler shift at different altitude for a 2GHz signal***

| Altitude (km) | Maximum Doppler Shift (kHz) |
|---|---|
| 800 | +/- 49,7 |
| 1500 | +/- 47,4 |
| 10000 | +/- 33 |

- Phase noise for non-regenerative (=bent-pipe) satellites only. In this case, the signal from the terminal (in S-band) has to be frequency shifted before being retransmitted towards the feeder in the FSS band, and vice-versa. This analogue frequency conversion inevitably creates phase noise.

- Non-linear distortion. This is induced by the on-board power amplifier, driven close to saturation for power consumption issues

## 2.3 Satellite channel characteristics

Since narrowband signals are considered, time dispersion effects can be neglected. In [1], Perez-Fontan proposed a three-state channel model, corresponding to line-of-sight (LOS), intermediate shadow and deep shadows conditions. Within each state, the received signal follows a Loo distribution [2], meaning that the signal is the sum of the direct signal and a diffuse multipath component. The direct signal is log-normally distributed while the diffuse multipath component follows a Rayleigh distribution. The direct signal variations are due to non-uniform receive antenna patterns and changes in mobile orientation with respect to the satellite [3].

The received signal is therefore statistically characterized by the mean and variance of the direct signal component, and by the mean power of the multipath component. Databases are

provided in [4], [5] and [6] as function of the elevation, considered area (urban, sub-urban, open…) and different receiver antenna directivity (hand-held and car-roof antennas).

A two-state channel model is considered in [7], not necessarily corresponding to LoS and non-LoS conditions. Within each state, the received signal is also the sum of a direct path and a multipath component, following therefore a Loo distribution. A versatile selection of statistical parameters is proposed in order to better correspond with reality.

## 2.4 Radio interface survey

### 2.4.1 Low Power Wide Area Networks and 5G

In the 90s, digital communications for telephone were introduced with the 2G of wireless telephone technology. It already included data services such as text messages, allowing users to exchange encrypted text, pictures and multi-media.

Now that the 4G (also referred to as LTE) is deployed almost worldwide [8], with peak data rates up to 1 giga-bits per second (Gbps), the 5G is considered. However, this next generation is not only predicted to increase the data rate, but also to include several new use cases [9], such as M2M communications and the IoT.

The IoT is the concept that every-day life objects should be connected to the Internet. The notion of connected object includes many things such as cellphones, sensors, wearable devices, components of machines … The concept also relies on the aspect that enabling the technology will unveil new, unexpected applications. Several billions of objects are expected to be connected [10], with an estimation of a ratio of connected devices per person above 6 for 2020 [11]. While most of the connections are done using cellular networks or legacy networks such as WiFi or Bluetooth, there is a gap between local wireless networks and cellular networks that needs to be filled. This is the problematic addressed by the LPWA networks. Out of the 25 billions of estimated connections for the IoT, more than 10% is expected to be LPWA connections [10].

4G communications are said to be synchronized. This communication is continuous, and induces overhead in the communication. One of the drawbacks of the procedure is when the device does not transmit nor emit a large quantity of packet. If for example, the device communicates with the base station during 1% of the time in one day, the synchronization procedure was on-going and useless for 1% of the time, inducing a waste of energy and spectrum resource. The energy waste happens at the device and base station level, as the radio was on without the necessity of sending data packets, and the spectral waste corresponds to the useless exchanges of synchronization packets, which polluted the transmission channel.

For these recent cellular networks, the concessions in terms of coverage and energy and spectral efficiency are accepted, as one of the main concerns is the QoS offered to the users. Low latency, high data rate and good coverage can be for example main criterion for user's satisfaction. The IoT introduces a new type of interaction: M2M communication. In M2M, the user is assumed to have no interactions in the communication. An example could be a sensor network, made of a numerous amount of sensor which communicate data to a cluster through a gateway, and the user only access the post-processed information computed by the cluster. This changes the requirements for the network, and extent the number of possible applications. It is accepted that legacy cellular network will still be a solution for some applications (for example, non-energy constrained problems which require high data rate), but new applications emerge with new requirements.

A typical example is smart-metering of water consumption. This application requires a solution on battery, preferably with long life duration to avoid frequent changes. When a rural situation is considered, a large coverage for the base station is required. This is also a financial benefit for the network access provider, as reducing the total number of base stations reduces its cost. The water metering sensors only send little information (few bytes of data, for example the consumption and the date), and they do so only once a week or once a month: the data rate over the period is very low. The use of a cellular network may be inefficient due to the large amount of overhead required for synchronization: a sporadic access is preferred, where the node enters into a sleeping mode after data transmission. The coverage offered by the cellular network may also not be large enough: a wider cell range should be considered. This simple example illustrates the need for a new type of network, the LPWA network. These networks are commonly characterized by some key features [12]:

- Long range communication, allowing a reduced number of base stations deployment compared to legacy cellular networks
- Long battery life for the devices, up to 10 years
- Low throughput communication
- Low cost device
- Massive number of devices connected to a single base station

### 2.4.2 Existing low power wide area industrial solutions

As more and more solutions required LPWA connectivity, some industrials went ahead and addressed the technical problematic with their own solution. More or less at the same time, the IEEE 802.15 and the 3GPP working groups developed standards to address the same problematic.

In this section, three major industrial solutions from Sigfox, the LoRa alliance and Ingenu are reviewed, as well as the standards 802.15.4k and the NB-IoT, part of a new release of the LTE standard.

#### 2.4.2.1 Proprietary Technologies

The two proprietary solutions presented here are industrial solutions: only few technical details are available, most of the documentation being marketing advertising. The ETSI nonetheless issued a specification for low throughput networks [13], and some backward engineering of the LoRa physical layer have been realized [14].

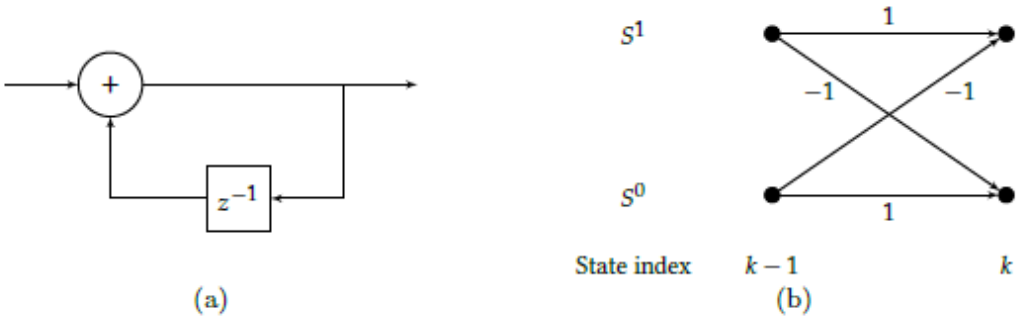


***Figure 2-3: Encoder (a) and trellis (b) of the DBPSK modulation. On the trellis, the input bit is labeled on***

#### *2.4.2.1.1 Sigfox*

Sigfox is a French company, created in 2010 and dedicated to IoT networks [15]. It is well known that the technology used by the company relies on narrow band signaling. Reducing the sensitivity level is equivalent to reduce the data rate $\mathrm{R} = \eta \mathrm{B}$, and this can done by reducing either the spectral efficiency of the technique, or the bandwidth. Narrow band signaling follows this second approach; a modulation with a relatively high spectral efficiency is used (without any channel coding), functioning at a high $\frac{\mathrm{E_b}}{\mathrm{N_0}}$, but the bandwidth $\mathrm{B}$ is low enough to ensure a satisfying sensitivity level.

The specification indicates a bandwidth of 100Hz and DBPSK modulation. This modulation is a memory modulation: the information is in the phase shifts. The modulation process can be represented by an encoder, given [REFFIG]. The output at time $k, x_k$, can be expressed using the two information bits $b_k$ and $b_{k-1}$ as $x_k = b_{k-1} \oplus b_{k1}$, with $\oplus$ the binary sum operator. The modulation can be also represented by a trellis, given in [REFFIG]. The input changes the state, and the output is the value of the state. In order to demodulate DBPSK and retrieve the Q information bits, the ML decoder would need to evaluate the likelihood of having each of the $2^Q$ possible sequences and search for the maximum, inducing an exponential complexity with $Q$. Instead, trellis decoding algorithm such as the algorithms used for convolutional codes can be used. The probabilities of transitions must be evaluated, while the probabilities of the states are observed. With $\boldsymbol{r}$ the received sequence of symbols, the LLR of the information bit at time $k$ can be expressed with

$$L(b_k) = log \frac{p(r_{k-1}|b_{k-1} = +1)p(r_k|b_k = +1) + p(r_{k-1}|b_{k-1} = -1)p(r_k|b_k = -1)}{p(r_{k-1}|b_{k-1} = +1)p(r_k|b_k = -1) + p(r_{k-1}|b_{k-1} = +1)p(r_k|b_k = -1)}$$

The DBPSK modulation with probabilistic decoding reaches a BER of $10^{-5}$ for $\frac{E_b}{N_0} = 9.9dB$, and its spectral efficiency is 1 bit/s/Hz. According to the definition of sensitivity

$$(P_{min})^{dB} = (\frac{E_b}{N_0})^{dB}_{min} + 10log_{10}(R) + 10log_{10}(k_B T 10^3)$$

and considering a bandwidth of 100Hz, the sensitivity is equal to $P_{min} = -143.7$dBm (without considering the noise factor of the receiver).

#### *2.4.2.1.2 LoRa*

The LoRa Alliance [16] is an association of companies which collaborate to offer a LPWA connectivity solution. The physical layer is based on a technology patented by the former company Cycleo, acquired by Semtech since. The original patent [17] describes a technology based on the emission of orthogonal sequences, chosen as chirps, hence the denomination CSSS. The use of chirp signals for communication has been explored before [18], and CSSS can be considered as an orthogonal modulation depending of the choice of the chirp sequence. The Zadoff-Chu sequences [19] are orthogonal as the circular autocorrelation of the sequence is zero for all nonzero delays: with a sequence of size M, a total of M delayed (or circularly shifted) sequences can be constructed, giving an alphabet of size M where each sequence is orthogonal to another thanks to the autocorrelation property. Alternatively, the process of chirp modulation can be seen as FSK modulation (i.e. an alphabet of pure frequencies), and then multiplying the complex symbols by the base chirp: spectrally, this spreads the power over all the carriers instead of exciting only one frequency. The Zadoff-Chu sequence is a CAZAC sequence, and has interesting properties such as constant envelope and good spectral localization.

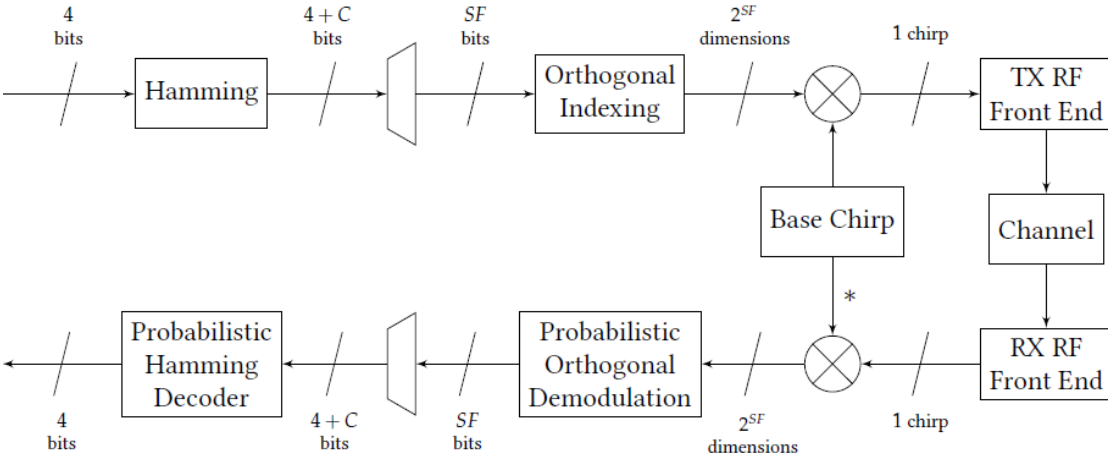


***Figure 2-4: The LoRa CSSS transmitter and receiver***

The TX and RX side of the LoRa modulation are given on the Figure 2-4. While the TX is described in the patent [17], we chose the RX side that performs the dual operations of the TX, with ML detection and decoding, as suggested by their technical document [20]. The FEC used is the Hamming code: $C$ parity bits are computed, with $C \in \{1,2,3,4\}$, where $C = 3$ corresponds to the regular Hamming code, while $C = 4$ is the extended version. The parity bits can also be punctured, i.e. not send, giving lower values for $C$. After encoding, bits are grouped into words of size $SF$ (which stands for SF, even is does not match the usual definition of the SF principle). Each group of bits is associated to one of the $2^{SF}$ orthogonal dimensions, and the result is multiplied by the base chirps in order to spread the signal on all frequencies.

At the RX side, the signal is de-spread by multiplying it with the conjugate of the base chirp. After this step, a classic orthogonal demodulation can be performed, in a coherent or non-coherent way. Each codeword of length $4 + C$ is then decoded, and the information bits are retrieved. The global spectral efficiency of the scheme is

$$\eta = \frac{4}{4+C}\frac{SF}{2^{SF}}$$

which is coherent with the use of an orthogonal modulation and the rate of the FEC scheme used.

The LoRa specifications indicate values of $SF$ from $6$ to $12$, and a signal bandwidth $B = 125$kHZ, $250$kHz or $500$kHz.

#### 2.4.2.2 Standardized technologies

In telecommunications, standards are defined in order to allow for various systems and operators to coexist. Without some level of standardization, communication between devices would be impossible. The proprietary solutions respect the regulations concerning bandwidth and duty cycles, but need to transmit in the unlicensed frequency band where anyone is free to transmit: interference with other users may be high. One of the benefits of using standardized solutions is the possible to use licensed band, where interference level is lower.

While the technology used by proprietary solutions is kept secret to ensure the monopoly of the inventor company for this very technology, standards are open access and simply define rules to follow for the design of the communication system. Anybody can then create its own system, compliant with the standard, but using its own algorithms for signal processing, demodulation, decoding or else. In this section, the definition of the rules for the PHY layer of two standards is reviewed.

##### *2.4.2.2.1 The IEEE 802.15.4k Standard*

The IEEE 802.15.4k is a standard for local and metropolitan area networks, and is part of the LRWPAN [21]. It aims at low energy critical infrastructure monitoring networks. This standard supports three PHY layer modes: DSSS with DBPSK or Offset-QPSK, or FSK. DSSS with DBPSK modulation is adapted to more constrained situations, and will be presented here. Standard specifications allow the use of a SF value $\boldsymbol{SF}$ from 16 to 32768, and packet lengths (before spreading) can be 16, 24 or 32 bytes.

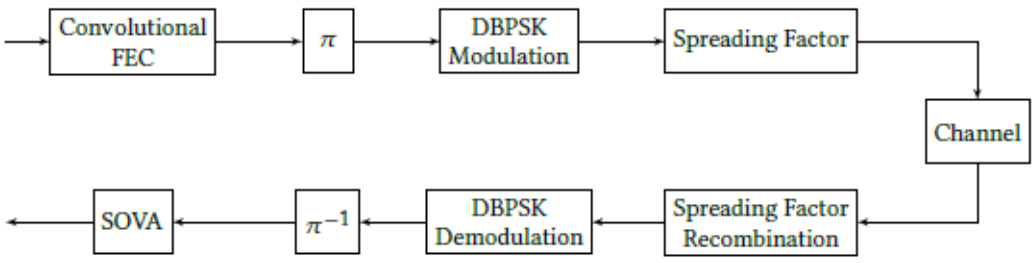


***Figure 2-5: The 802.15.4k specifications transmitter and receiver***

Block diagrams for transmitter and receiver are given in ***Figure 2-5***. The transmitter is composed of a FEC block, defined to be the convolutional code of rate 1/2, with generators polynomial [171 133] and constraint length k=7. After encoding, interleaving is done to ensure diversity at the reception side. The data is modulated using DBPSK and is ``repeated'' by the use of a binary direct sequence of size SF. The normalized spectral efficiency of the physical layer is

$$\eta_1 = \frac{1}{2SF}$$

The receiver executes the reverse operations of the transmitting side. After de-spreading the signal (executing the mean weighted by the elements of the binary direct sequence), we use a soft DBPSK decoder. Knowing how data was interleaved at the transmitter side, the de-interleaving operation allows the Soft Viterbi decoder to retrieve the information bits.

While the standard has been considered as a LPWA solution [22], the RPMA technique, developed by the US company Ingenu [23], is allegedly based on the 802.15.4k standard: its PHY layer is compliant with the standard. It uses the DSSS technique, and their specific access technique is described by the patent [24]. Regarding the physical layer, we will consider the exact same elements as the 802.15.4k standard, except the possible values for the SF, ranging from 64 to 8192.

#### *2.4.2.2.2 Narrowband LTE for IoT*

The 3GPPP consortium recently issued a standard for the NB-IoT [25]. This standard is actually a new release of the LTE standard [26], and includes 3 modes for IoT applications. Since it is an evolution of the LTE, it includes other elements of this standard, such as its channel coding procedure [27]. Some industrial group research teams also unveiled more about the NB-IoT standard, such as Nokia [28] and Ericsson [29]. The NB-IoT has two main modes: the DL and UL modes.

For the UL mode, the modulation can be chosen between BPSK and QPSK, and the FEC used is the [13 15] TC from the LTE standard [27]. The parity bits of the TC can be punctured, giving two possible rates for the channel code: 1/3 and 1/2 (when punctured). The message can be repeated up to 128 times, giving a processing gain at the receiver side.

For the DL mode, i.e. the connection from the base-station to the device, data is modulated using QPSK. The channel code used is a TBCC, with generator polynomials [133 171 165] [27], giving a rate 1/3. The use of TBCC allows the receiver (the device) to use a low complexity Soft Viterbi decoder, and the tail biting property avoids the needs to send extra bits to close the trellis. A repetition up to 512 can be applied.

As part of the LTE standard, the data must be modulated using OFDM signaling. For the DL, classic OFDM is assumed, while for the UL, both SC-FDMA and single carrier transmission are considered. Compared to OFDM, both SC-FDMA and single carrier offer a lower PAPR [30], which is interesting at the device level as it lowers the energy consumption of the PA.

The architecture of an OFDM/SC-FDMA transceiver is given on the Figure 2-6. Modulated symbols a gathered into groups of size $N_{DFT}$, and a DFT of the same size is applied on each group. The symbols are then mapped to $N_A$ carriers, and an iFFT of size $N_{FFT}$ is applied: while the mapping of the symbols was done in the frequency domain, the iFFT generates a signal in the time domain. After this step, a CP is inserted, i.e. the last $N_{CP}$ samples of a time

symbol (which contains $N_{FFT}$ samples) are added at the beginning of the symbol, giving a symbol with $N_{FFT} + N_{CP}$. At the receiving side, after removing the CP, a FFT is applied to recover the mapped symbols from the transmitter. The iDFT is then applied to the DFT blocks send at the first place, in order to recover the modulated symbols. SC-FDMA is a multiplexing technique, as several symbols are transmitted at different frequencies during the same time symbol. The DFT step can be seen as a type of pre-coding, and is omitted when OFDM signaling is considered.

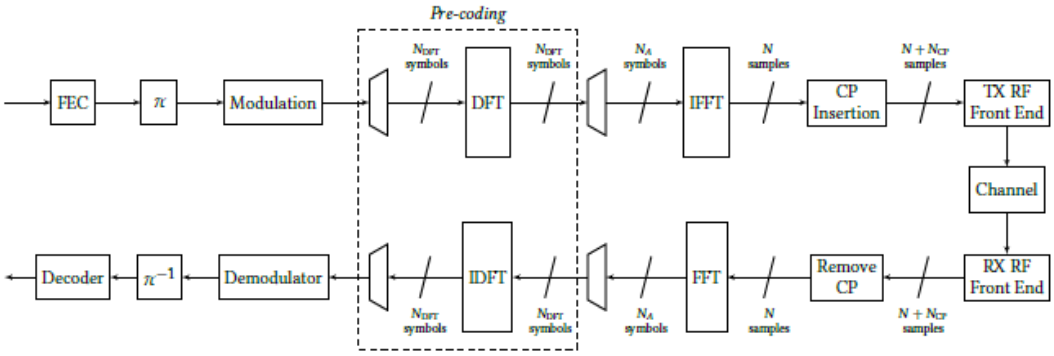


***Figure 2-6: The OFDM/SC-FDMA transmitter and receiver***

The value of $N_A$ is usually equal to $N_{DFT}$, equal to 12, 6 or 3. The carrier spacing in LTE being 15kHz, the bandwidth of 12 carriers is equal to 180kHz. When only a single carrier is used, the bandwidth can be chosen equal to 15kHz or 3.75kHz.

The spectral efficiency of the NB-IoT scheme is given by

$$\eta = R_c \frac{\eta_{mod}}{SF}$$

where SF is the factor of repetition, $R_c$ the coding rate and $\eta_{mod}$ the spectral efficiency of the modulation.

### 2.4.3 Performance comparison

The parameters of the different technologies presented previously that minimize the sensitivity are summarized in Figure 2-7. For Sigfox, only one mode is available, but for every other technique, the parameters of the mode giving the lowest spectral efficiency are indicated. The bandwidths, data rate, sensitivity levels and the band used are also given. In order to obtain the estimated sensitivity levels, simulations of the different schemes under an AWGN channel were performed, and the $\frac{E_b}{N_0}$ required for a BER of $10^{-5}$ is integrated in the sensitivity formula along with the data rate of the technique.

Whatever the technique used, extremely low levels of sensitivity can be reached, at the expense of a very low data rate. Naturally, these values do not include the possible implementation performance loss or the noise factor of the receivers. Probabilistic decoding and MAP decoding for the TC have been selected, while industrial transceiver may choose different implementations. However, this comparison gives the extreme limits of each technology concerning the reachable sensitivity.

| | Parameters | $\eta$ | Bandwidth | R | Band | Sensitivity |
|---|---|---|---|---|---|---|
| *Unit* | - | $bits{\cdot}s^{-1}{\cdot}Hz^{-1}$ | *Hz* | $bits{\cdot}s^{-1}$ | *MHz* | *dBm* |
| Sigfox [40] | - | 1 | 100 | 100 | 868 (ISM) | −144 |
| LoRa [47] | $SF = 12\ C = 4$ | $1.4 \cdot 10^{-3}$ | 125,000 | 183 | 868 (ISM) | −147 |
| RPMA [50] | $SF = 8192$ | $6.1 \cdot 10^{-5}$ | $1 \cdot 10^{6}$ | 61 | 2,400 (ISM) | −150 |
| NB-IoT (DL) [52,55] | QPSK, $R_c = 1/3$, $SF = 512$ | $1.3 \cdot 10^{-3}$ | 180,000 | 234 | ? (Licensed) | −146 |
| NB-IoT (UL) [52,55] | BPSK, $R_c = 1/3$, $SF = 128$ | $2.6 \cdot 10^{-3}$ | 3,750 | 9 | ? (Licensed) | −163 |

***Figure 2-7: Parameters of the different modes which minimize the sensitivity level, for all the considered techniques***

On Figure 2-8, the spectral efficiency versus the $\frac{E_b}{N_0}$ required for a BER of $10^{-5}$ for each technology has been represented, along with the channel capacity, given by (see Annex 1)

$$\frac{E_b}{N_0} = \frac{2^{\eta_{max}} - 1}{\eta_{max}}$$

Along with the lowest possible spectral efficiencies, the performance characteristics for the highest spectral efficiencies are also given for each technology, for illustration. It should be reminded that this representation is normalized with the bandwidth: while Sigfox appears far from the channel capacity, this solution still reaches low levels of sensitivity following its narrow band approach. For all the other technique, low sensitivity is reached by decreasing the spectral efficiency, and the $\frac{E_b}{N_0}$ performance varies from one technology to another. The NB-IoT approach, as it uses a TC, is the closest to the channel capacity, with a gap of approximately 2.6dB for its lowest spectral efficiency point (note that an interleaver size Q=1000 was used for this performance), while Sigfox is the farthest with a gap of ≈10dB. One should consider that complexity of the schemes is different, as the receiver needs to compute turbo decoding for the NB-IoT case. However, since this is the UL mode, the receiver in this case is a base station, which can be considered to have a large computational capacity: the cost of complexity increasing due to the use of a more sophisticated FEC can be paid by the receiver side. The difference of performance in $\frac{E_b}{N_0}$ should not be interpreted directly as the difference in sensitivity, since the bandwidth and spectral efficiencies of Sigfox versus NB-IoT are not similar. However, a data rate of 104bits/s can be achieved by using the NB-IoT with parameters $SF = 12, R_C = 1/3$ and a bandwidth of 3.75kHz and BPSK modulation. The spectral efficiency in this case is equal to $\eta = 0.027$bits/s/Hz, and with a $\frac{E_b}{N_0} = 1$dB, the sensitivity for this case is -153dB. **This means that for a same data rate, the NB-IoT with these parameters uses 37.5 more bandwidth and more complexity to**

**achieve a gain of 9 dB in sensitivity versus the Sigfox solution**. Other comparisons could be made, but the choice of one solution versus another is always a matter of compromise on the bandwidth, time duration of the signal, and complexity. It is however straightforward that all solutions follow the same strategy: reduce the data rate.

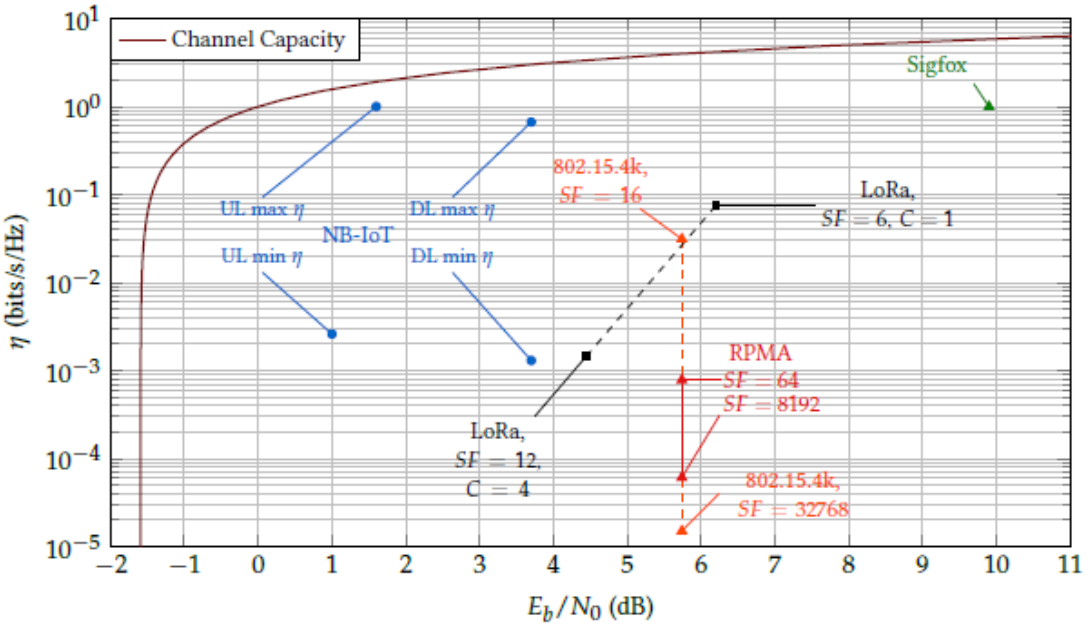


***Figure 2-8: Performance at BER=10e-5 of various LPWA solutions versus their spectral efficiency.***

The design of a new LPWA PHY layer is a critical issue for the new generation of IoT networks, as a large amount of connected devices are expected to need this type of connectivity solution in the coming years. Industrial solutions exist and standardization is in the process. The main strategy to reach low sensitivity levels is clearly to reduce the data rate, either by reducing the bandwidth or the spectral efficiency of the technology used. When considering the minimum achievable Eb/N0 according to the channel capacity as defined by Shannon versus the various LPWA solutions, an important gain in energy efficiency has not been yet achieved. The ultimate limit (Eb/N0)lim = 1.59dB can be approached only by solutions that have a relatively low spectral efficiency. However, lowering the spectral efficiency is not sufficient to getting closer to the limit: most solutions are 5dB away from the (Eb/N0)lim. Only the use of Turbo coding solution provided by the UL NB-IoT standard is the closest to (Eb/N0)lim, at the expense of an increased complexity at the receiver side: the transmitter (i.e. the node) complexity is kept low to ensure low consumption. More sophisticated reception algorithms should be considered in order to achieve a gain in energy efficiency. The choice of waveform is also a critical matter as it impacts the energy efficiency and the PAPR of the technique, and a constant envelope technique is preferred in order to release some constraints on the transmitter's PA. This constraint is particularly important to consider if a common technology has to be defined for terrestrial and satellite network.

Therefore, we propose, in the next section a new physical layer for IoT, compatible with the current implementation of NB-IoT, with equivalent performance and reducing PAPR.

# 3 Technical enablers analysis

## 3.1 Waveform design

### 3.1.1 Proposed IoT scheme for beyond 4G terrestrial and satellite networks

An interesting option to combine both $\frac{E_b}{N_0}$ and spectral efficiency reduction is the use of M-ary orthogonal modulations. Even though the transmitter has a low complexity, most of the current LPWA solutions rely on other Forward Error Correction (FEC) codes, and a potential improvement can be done by introducing more sophisticated receiver algorithms. The use of orthogonal alphabet and coding in the same transmit process combined with a turbo receiver is proposed here. To manage PAPR and therefore power consumption, we propose to combine FSK orthogonal modulation with a simple accumulator code. This modulation is an interesting choice as its constant envelope property provides a power efficient solution regarding the transmit power amplifier. The use of pure frequency waveforms also leads to robustness through frequency-selective multipath channel and can be easily implemented on top of an OFDM transmitter. We denote Coplanar Turbo-FSK this new modulation scheme.

#### 3.1.1.1 Turbo FSK description

This scheme allows for a better use of redundancy than in pure repetition scheme, and achieves an interesting energy efficiency gain. The transmitter low complexity makes it suitable for uplink communication in the LPWA context.

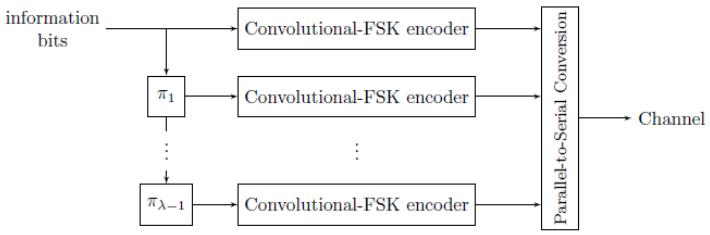


***Figure 3-1: The Turbo-FSK transmitter***

Transmitter architecture is given in Figure 3-1 . The structure is composed of λ stages, each one encoding an interleaved version of the input bits. Information bits are gathered into P groups of r bits, and Convolutional-FSK encoding is applied, as described Figure 3-2.

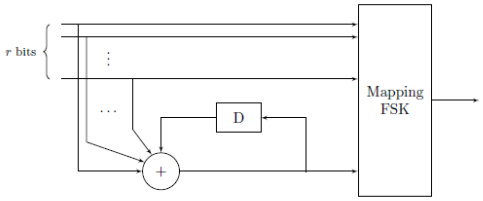


***Figure 3-2: The convolutional-FSK encoder.***

For every group of r bits, parity is computed and accumulated in the memory. The r+1 bits are then mapped to a codeword of the FSK alphabet, which size is M = $2^{r+1}$. Thanks to the accumulator, every consecutive symbol is linked to the previous one. The output of each encoder is then a set of P FSK codewords: this scheme mixes coding and modulation in the same process. A Parallel-to-Serial Conversion is then done to send the FSK codewords through the channel. The spectral efficiency is defined by

$$\mu = \frac{log_2 M - 1}{\lambda M}$$

The receiving side, depicted in Figure 3-3, consists of Serial-to-Parallel Conversion, to reconstruct the λ stages emitted at the first place.

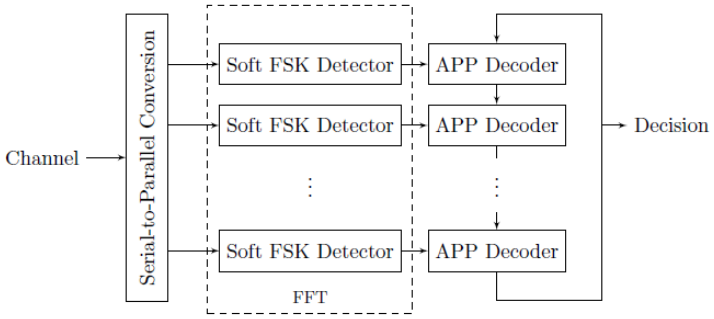


***Figure 3-3: The Turbo-FSK receiver.***

A Soft FSK Detector is used to determine the probabilities of each possible codewords. This step can be done using the Fast Fourier Transform (FFT) algorithm. These probabilities are then fed to the APP decoder, which will use them as channel observation, while output of the other decoders will be used as a priori information. BCJR algorithm is used to decode the trellis. Orthogonality of the transmitted codewords is one of the key features of this scheme, which offers a great performance gain compared to simple repetition schemes. Detailed explanations about the transmitter and the receiver's computations can be found in [32]. A straightforward implementation of the transmitter can be done using FFTs as depicted in [33].

#### 3.1.1.2 Coplanar-Turbo-FSK

In order to increase the spectral efficiency of the technique, a hybrid modulation alphabet mixing FSK modulation (orthogonal component) and PSK modulation (linear component) is proposed. The scheme is denoted Coplanar-Turbo-FSK. The constant envelope amplitude is preserved while the spectral efficiency is increased

34][35]. It has been demonstrated that the choice of the PSK is the optimal modulation in the sense of minimizing the channel capacity gap to the Shannon limit. In [36], it has been demonstrated the benefits of Coplanar-Turbo-FSK signaling on typical terrestrial channels with respect to NB-IoT waveform.

In this work, we discuss the integration of Coplanar-Turbo-FSK in the OFDM framework. We demonstrate the possibility for the proposed techniques to use a transmitter and a receiver based on an OFDM-like architecture. While classical OFDM based modulation exhibits important envelope variations, a known effect for this modulation, the proposed techniques offer a constant envelope signal, which improves the efficiency of the PA. An illustration of the proposed transmitter is depicted in Figure 3-4.

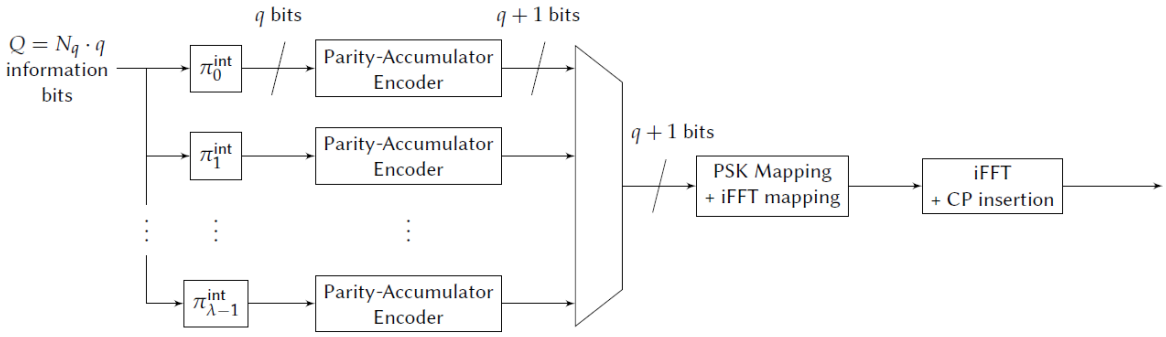


***Figure 3-4: Coplanar-Turbo-FSK transmitter architecture when combined with OFDM framework.***

### 3.1.1.3 Performance assessments

Three schemes are considered: OFDM modulation, where QPSK symbols are mapped on the used carriers, SC-FDMA, where a pre-coding is applied and FSK modulation. The use of the turbo code [13 15] as channel coding is considered. Each scheme is integrated into the FFT-based system, in order to fit the context of OFDM waveform framework. OFDM and SC-FDMA are the waveforms considered for NB-IoT. The comparisons concern practical aspects commonly used to describe a system. Three aspects are considered: the variation of the envelope of the signal at the output of the transmitter and the performance of the system under various channels. For each aspect, the performance of every techniques is assessed using specific parameters. For a fair comparison, the schemes are always compared with the same spectral efficiency and spectral occupation, 180KHz. The same number of information bits is sent over the same Time-Frequency allocation. The rate matcher of each scheme will then puncture or repeat some bits/codewords.

There are many possible configurations for the 3 schemes. In order to restrict the study, some parameters are kept constant for all the schemes. As all the schemes were presented associated with the same architecture, the parameters for this architecture can be taken equal for all the schemes. The parameters are chosen as corresponding to the mode 1.4MHz of LTE (NB-IoT).

The packet size (or information block size) is set to 1000 bits. For the rest of the parameters, two scenarios are considered: a low throughput 8.24kps and a high throughput 46.68kps. In addition to the restriction of the choice of parameters in two scenarios, several assumptions

are made. The first assumption is the ideal synchronization. There is no carrier or clock frequency offset, and no phase noise or timing offset.

#### *3.1.1.3.1 Instantaneous-to-Average Power Ratio (IAPR)*

The variations of the envelope of a signal can be measured through the computation of the IAPR. This measure is very useful for evaluating the constraints for the power amplifier (PA). It is more relevant than the measure of the peak to average ratio as it considers all the samples of the signal (and potentially, the samples that could reach the non-linear region of the PA) Having large variations will result in the necessity of having a highly linear PA, i.e expensive and energy inefficient.

The IAPR is measured from the time signal which is sent through the channel.

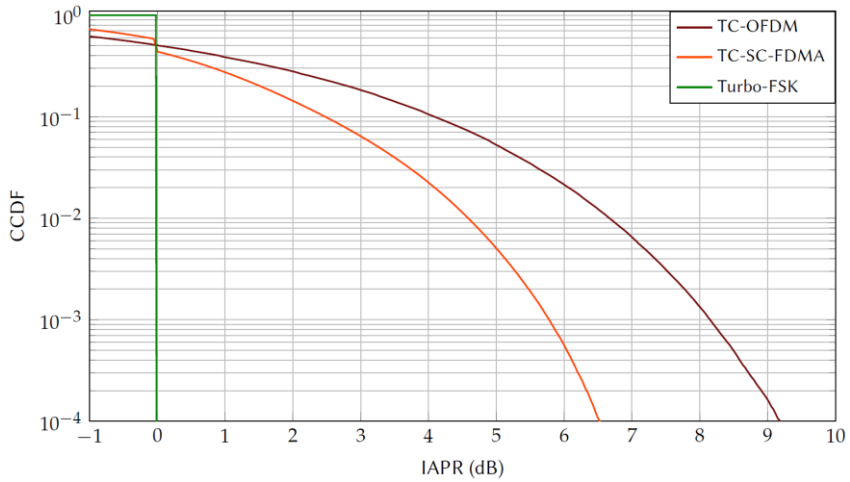


***Figure 3-5: IAPR comparison.***

The CCDF of the IAPR's is depicted in Figure 3-5. The OFDM has the largest variations and exhibits a probability of 10e-3 to have an IAPR larger than 8dB. The \SC-FDMA shows a 2dB improvement in its variations, thanks to the use of pre-coding. The proposed Turbo-FSK have an IAPR of 0dB, as this scheme uses the FSK modulation which has a constant envelope.

The measure of the IAPR clearly emphasizes the major benefit of FSK signalling, its constant amplitude property. It guarantees an IAPR equal to 0dB for all samples making particularly interesting for low power consumption communication and satellite communication. On the opposite, the IAPR of OFDM exhibits large variations, a well-known drawback of the technique.

#### *3.1.1.3.2 Performance on AWGN channel*

Regarding performance of the Coplanar-Turbo-FSK with respect to Turbo code based scheme on Additive White Gaussian Noise (AWGN), the Signal to Noise Ratio (SNR) to reach low Packet Error Rate (PER) is coarsely the same. As an example we depict in Figure 3-6, the required SNR to achieve a PER of $10^{-2}$ for various throughput and two sizes of payload, namely 256 and 1024 bits. For Coplanar-Turbo-FSK, we assume 32 sub-carriers

and M-PSK modulation, M={4,8,16,32}. Regarding the Turbo-code we consider the LTE coding scheme of rate 1/3 with QPSK modulation and repetition coding. The simulation results show a small gain, tenths of dB, considering the proposed scheme.

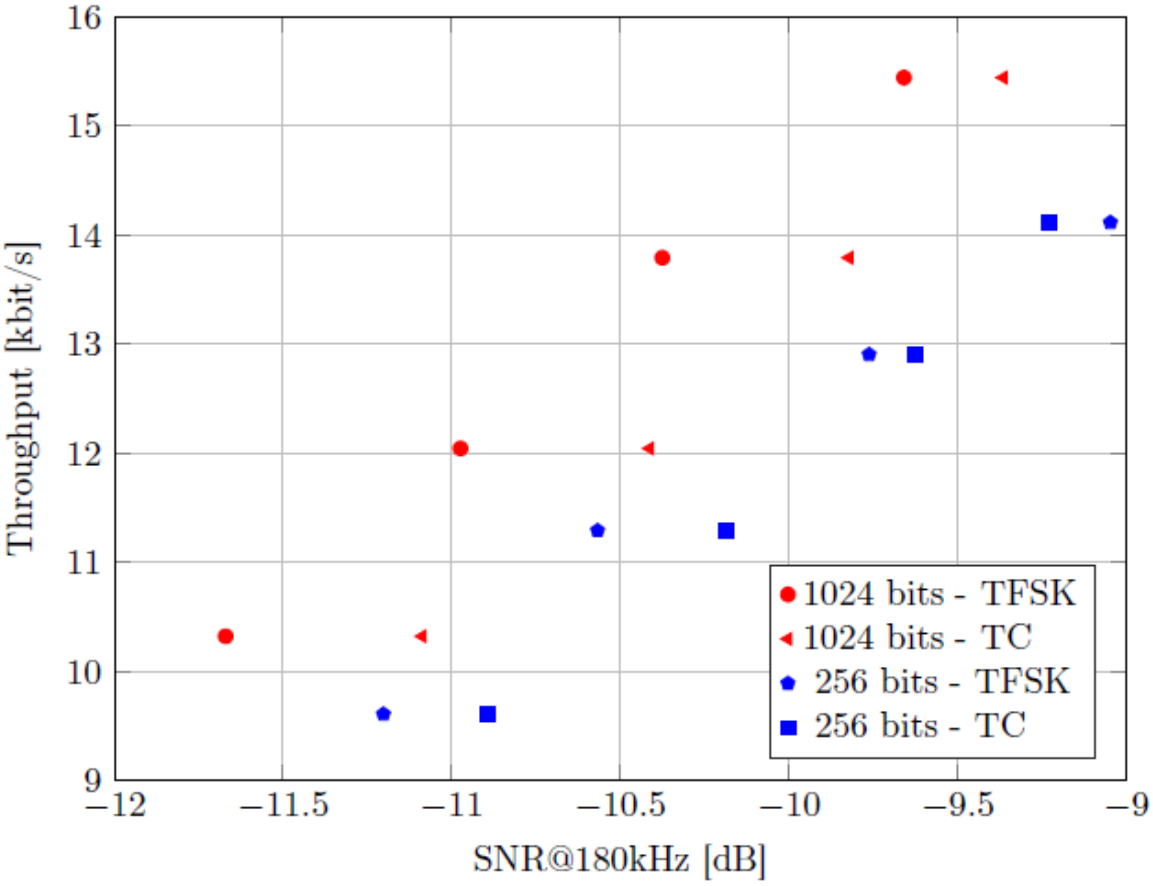


***Figure 3-6: AWGN performance comparison of Coplanar-Turbo-FSK (labeled TFSK) with 32 sub-carriers and M-PSK, M={4,8,16,32}, λ = 4 and LTE turbo coding scheme (labeled TC)***

In Section 3.2 we propose to illustrate how to design a frame structure compatible with the proposed scheme and we assess performance on a typical satellite channel.

#### *3.1.1.3.3 Performance on Frequency selective channels*

When considering frequency selective channels, multiple models can be selected. For our study, Rayleigh fading is considered, i.e the complex gains of the various paths follow a circular complex Gaussian distribution and the modulus of the complex gain is Rayleigh distributed. The 3GPP organization defines several fading profiles. For our study, the ETU fading profile is considered. A profile is defined by the delays and the average attenuation of the different paths. Generating the channel consists in generating a \FIR filter. The physical multi-path channel with analog delays must be interpolated to correspond to the considered

sampling frequency. When considering a 1.92MHz sampling frequency, the physical paths of the channel give a total of 14 samples for the channel coefficients.

The delay spread of the channel is the maximum delay incurred by the channel. For the ETU profile, this delay spread is equal to 5us. The coherence bandwidth of the channel is the bandwidth over which the channel is correlated. The channel can be considered frequency flat over a bandwidth small compared to the coherence bandwidth. For the ETU profile, the coherence bandwidth is equal to 200kHz.

For the simulation, the channel is considered constant over the whole duration of the transmitted signal. In order to compare the schemes, the performance over a fixed number of channel realizations is computed. Each realization having its own gain, the SNR is estimated at the input of the receiver. In the presented figures, the average SNR over all the realizations is presented on the horizontal axis. All the compared techniques experience the same realizations of channel. A large number of realizations is computed and perfect CSI is considered.

The performance of the different schemes for the low throughput scenario is depicted in Figure 3-7. For this scenario, the performance of OFDM and Turbo-FSK are almost similar. The OFDM performs 0.2dB better than Turbo-FSK for a PER of 10e-2. The SC-FDMA shows the worst performance. This can be attributed to the ZF equalizer, which is known to perform poorly under frequency selective channels.

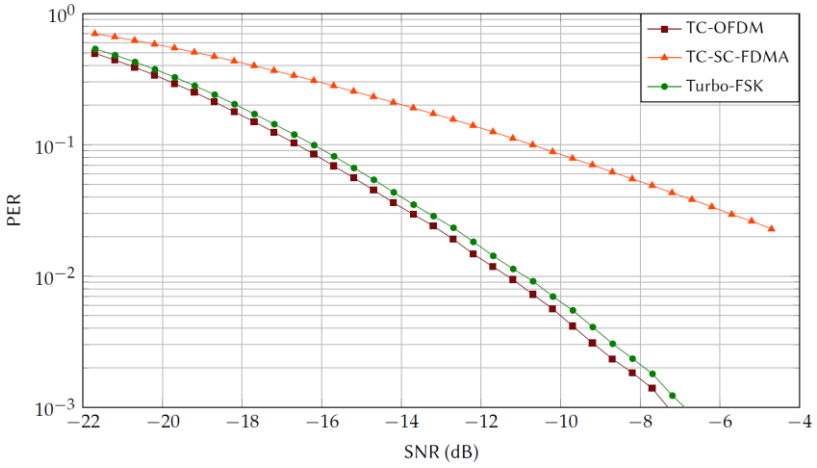


***Figure 3-7: Performance for the low throughput scenario under the static Rayleigh fading channel with an ETU fading profile.***

Overall, all the schemes demonstrate a frequency diversity which allows them to perform well under this type of channel.

The performance when considering the high throughput scenario is depicted in Figure 3-8. As in the other scenario, the SC-FDMA shows poor performance due to the use of the ZF equalizer. The Turbo-FSK shows a 1.8 dB loss compared to OFDM. This effect is not observed in the low throughput scenario, which may suggest that the use of a higher spectral efficiency magnified the difference.

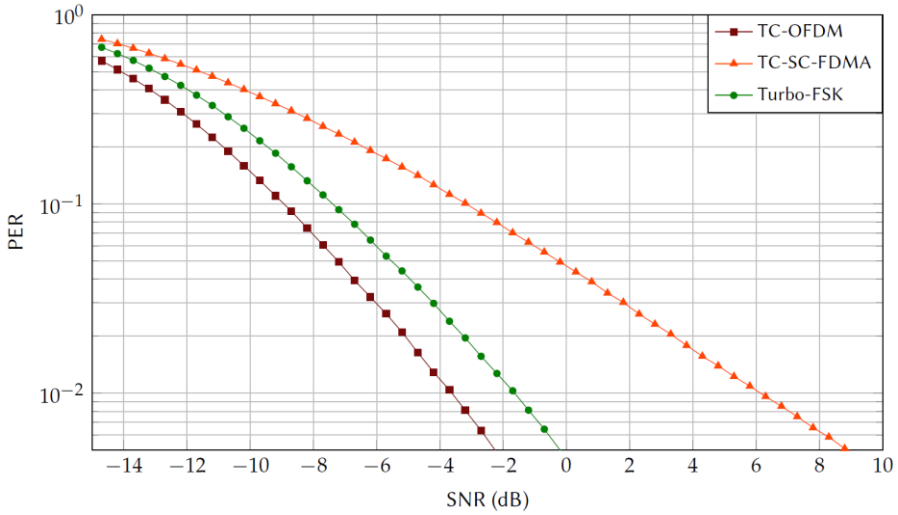


***Figure 3-8: Performance for the high throughput scenario under the static Rayleigh fading channel with an ETU fading profile.***

#### *3.1.1.3.4 Synthesis*

The performance of each scheme is summarized in a 5-point axis representation, in Figure 3-9. The five axes represent: how constant is the envelope (which gives a low value for large variations and vice versa), the performance under the AWGN channel relative to OFDM combined with Turbo coding, under the Rayleigh fading channel with ETU fading profile, with both static and mobility conditions and finally the implementation efficiency (complexity of the receiver)

For the low throughput scenario, the Turbo-FSK offers the best compromise. Its constant envelope property distinguishes its performance from OFDM and SC-FDMA. Eventually, the SC FDMA has a performance similar to the OFDM in AWGN and in mobility (because of the high redundancy of the scheme for this scenario) and less variations of envelope, but the use of the ZF equalizer does not allow the scheme to perform well under static ETU conditions. Moreover the precoding-FFT algorithm required at the receiver increases the complexity.

The OFDM and the SC-FDMA have the same performance when considering the high throughput scenario. For both schemes, increasing the throughput was done by reducing only the repetition factor. For Turbo FSK, considering a higher throughput was done by changing intrinsic characteristics of the schemes. These modifications deeply impact the performance and complexity, and also emphasize the differences in the choice of the orthogonal alphabet.

When it comes to choice, we propose to study the Turbo FSK for low throughput and energy constraint communication and move to SC-FDMA for higher throughput at the price of lower energy efficiency (mainly to the Transmitter PA that needs 4 to 6 dB back-off). Therefore, the use of a “new mode” based on Turbo-FSK, allowing for constant envelope and PA

optimization and enabling good performance on typical terrestrial channel model, can bridge the gap in the adaptation of a common technology for cellular IoT. Seamless adaption to satellite and terrestrial network is possible.

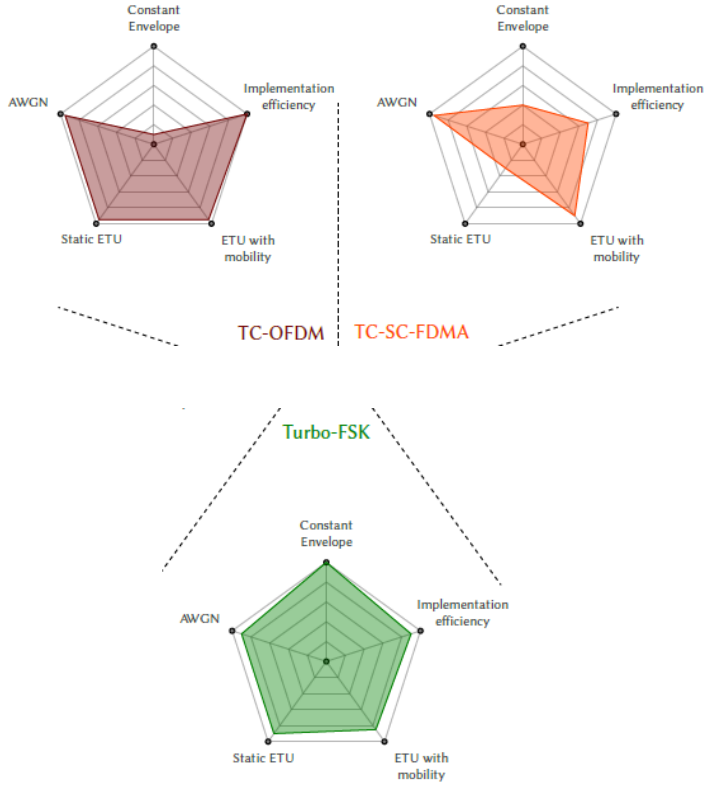


***Figure 3-9: Performance of the compared schemes.***

## 3.2 Frame structure

In order to keep a flexible frequency and time block allocation, a preamble based burst approach is considered. Synchronization and channel estimation is performed using the training sequence. Its structure has been defined and is illustrated in Figure 3-10.

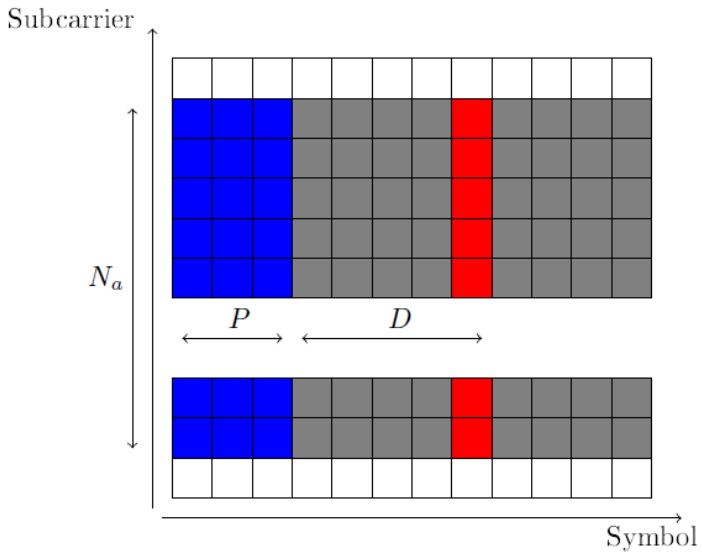


Figure 3-10: Considered radio frame structure. Blue boxes are for sub-carriers dedicated to synchronization preamble, gray boxes for payload and red boxes for pilots sub-carriers.

It is composed of a preamble of duration P OFDM symbols (P is set to 3 in the Figure 3-10) of $N_a$ sub-carriers. The preamble has been designed to accurately detect the start of the burst and gives an estimate of the channel frequency offset. The payload part is composed of pilot carriers spaced every D active carriers (D is set to 5 in the Figure 3-10). The payload structure has been designed to give an estimate of the channel frequency response and to track its evolution within the total duration of the transmission.

The preamble and pilot carriers are Zadoff-Chu (ZC) sequences [37] defined in frequency domain as follows:

$$Z[k,t] = \alpha(t)e^{-j\pi\frac{k^2}{N_a}}, \forall k \in [0, N_a - 1]$$

where $\alpha(t)$ modeled a scrambling function, i.e $\alpha \in \{-1,1\}$. The time domain signal, after the $N_{FFT}$ points inverse FFT is defined as follows[1]:

$$z[\tau,t] = \alpha(t)\sum_{k=0}^{N_a-1} e^{-j\pi\frac{k^2}{N_a}} e^{2\pi j\frac{k+\nu}{N_{FFT}}\tau}$$

where $\nu$ modeled the allocation of the sequence within the frequency grid.

One drawback of this sequence (up sampled by the iFFT transform) is the relative high PAPR with respect to Coplanar-Turbo-FSK (0dB PAPR) when $N_a \neq N$. For example the PAPR of a ZC sequence of length 32 is 2.6dB for $N_{FFT}$=512 as depicted in Table 3-1. Therefore

[1] We assume OFDMA, and an allocation of $N_a$ sub-carriers within a frequency grid of size N sub-carriers

designing low PAPR sequences is necessary to keep the constant envelope property of the proposed waveform.

In this work we propose a simple method to build low PAPR sequence. First, as mentioned previously, the considered SNR reach a PER of $10^{-2}$ is quite low. So it is possible to design and optimize a sequence composed of the ZC sequence and a noise vector X in such a way that the resulting PAPR is low and the Signal to Interference ratio (SIR) on each sub-carrier $\rho$ is greater than a given value. The optimization problem can be expressed as follows:

$$\begin{aligned} \underset{X}{\text{minimize}} \quad & \max\left(\frac{|z[n]|^2}{\frac{1}{N_a}\sum_{n=0}^{N_a-1}|z[n]|^2}\right) \\ \text{subject to} \quad & \frac{1}{|X[k]|^2} > \rho, \forall k \end{aligned}$$

where z[n] is :

$$z[n] = e^{j2\pi\frac{n\beta}{N}} \sum_{k=0}^{N_a-1} (Z[k] + X[k])\, e^{j2\pi\frac{nk}{N}}$$

The optimization problem is not convex and therefore an iterative solver has been used. Results are depicted in Figure 3-11. When the SIR constraint is 20dB and for $N_a$=32, it is possible to find a sequence with only 1.43dB PAPR, so a gain of 1.2 dB with respect to the noise-free ZC sequence. If the SIR is reduced to 7dB, the PAPR is equal to 0.7dB.

| $N_a$ | 32 | 16 | 8 |
|---|---|---|---|
| PAPR(Z) [dB] | 2.6306 | 2.6171 | 2.5372 |
| PAPR(Z+X) [dB] $\rho_{dB} = 20$ | 1.4395 | 1.6408 | 1.8008 |
| PAPR(Z+X) [dB] $\rho_{dB} = 15$ | 1.3883 | 1.4917 | 1.7772 |
| PAPR(Z+X) [dB] $\rho_{dB} = 7$ | 0.7180 | 0.8149 | 1.0711 |

***Table 3-1 - PAPR of ZC sequence when $N_{FFT}$=512***

As the level of interference is smaller than the target noise level, one can assume a limited performance loss. This effect will be studied in the next section.

ZC sequences have been widely used as synchronization sequences in current wireless communication systems due to their good autocorrelation properties [37][38]. Moreover, the cross correlation of a ZC sequence and itself plus a Carrier frequency offset (CFO) also gives a shifted peak in the time domain. This property can be useful to estimate a CFO during a preamble. The ambiguity function of defined as follows:

$$\mathcal{A}(f,t) = ||\sum_{k} z^*[k-t]z[k]e^{j2\pi ft}||^2$$

can be computed to demonstrate this property. We have depicted in Figure 3-11 the ambiguity function for various value of $\rho$ from 7dB to $\infty$ dB (no noise on sequence).

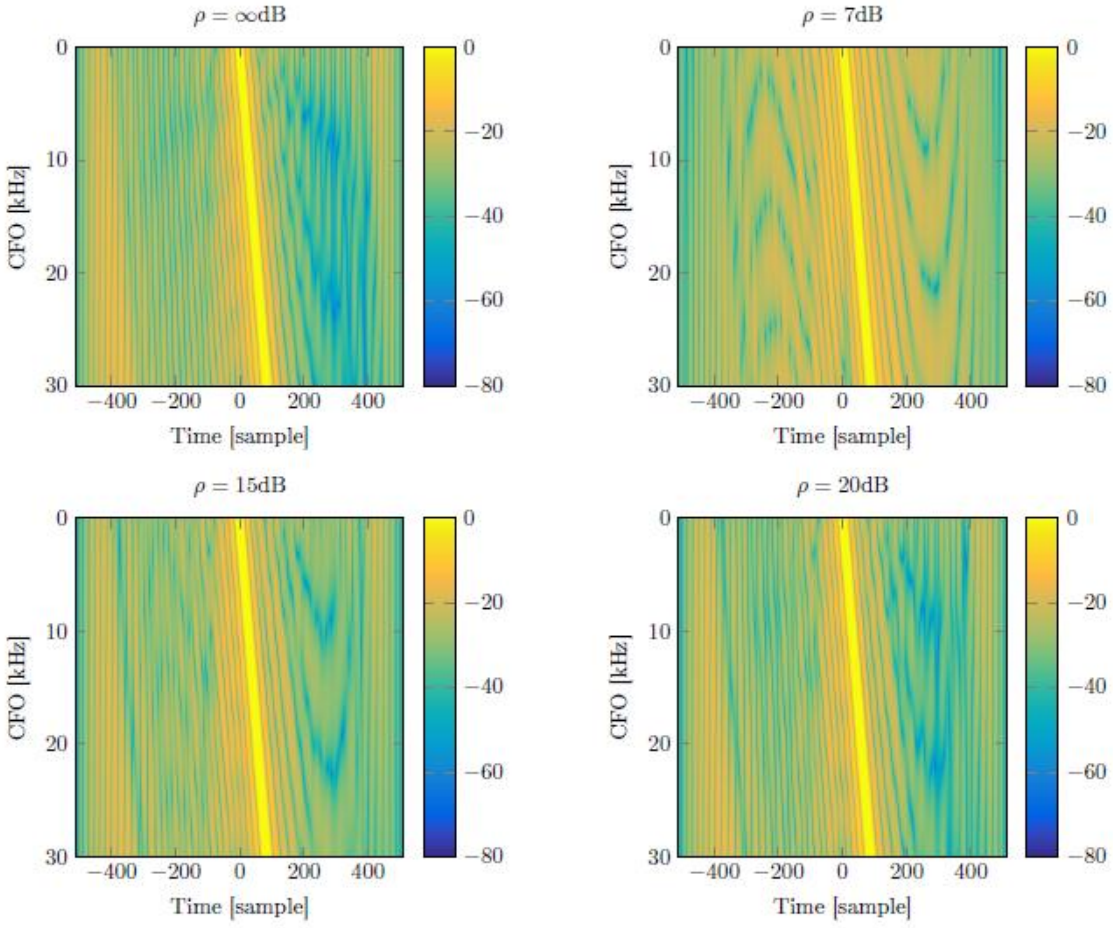


***Figure 3-11: Ambiguity function of various sequence, with different .***

First of all, the position of the maximum value shifts with the CFO. This property is interesting to jointly estimate the beginning of a frame and the CFO (see [35] for instance). Secondly, introducing noise on the sequence does not modify the behavior of the ambiguity function, even with a level of 7dB. It means that the proposed scheme does not destroy the properties of the sequence making the proposed scheme very interesting when a low PAPR is needed.

## 3.3 Radio protocol impact

There are several specificities to satellites and/or HAPS that require some 5G systems adaptations in order to fully integrate the satellite components. These changes are summarized in Table 3-2, and impact the different layers of 5G systems, and are not specific to narrowband IoT services exclusively.

At the physical layer, Doppler shift, which is especially high for LEO satellites (up to about ±50kHz) , necessitates to apply margins to avoid out of blocks transmissions. Considering

180 kHz block bandwidth, the terminals shall transmit only in 80 kHz if no compensation is applied. Since a large number of terminals are transmitting simultaneously, it is expected that the full 180 kHz block bandwidth is used, so that no capacity reduction occurs.

In the context of narrowband IoT, where only sporadic traffic is transmitted by a huge number of terminals, random access techniques should be used to avoid high signaling overhead. Moreover, it is then not necessary to cope with the difference in propagation delays between terminals, which are in the order of a few ms for satellite systems. A higher complexity is necessary at the gateway side to detect the received signals since collision may occur and frequency of signals is unknown.

Low PAPR modulations are usually preferable in order to drive the power amplifier onboard the satellite close to its saturation point. However, the amplified signal is here the concatenation of independent signals related to each resource block. Therefore, low PAPR modulations are not critical in the considered context.

A seamless handover between infrastructures is targeted as it uses the same 5G waveform with potential dynamic reconfiguration of the protocols and mechanisms to adapt to each technology.

***Table 3-2: Satellite/HAPS specifics implying modifications of 5G systems for satellite/HAPS operations***

| Satellite/HAPS specifics | 5G system impacted areas | Features to be adapted for satellite/HAPS operations |
|---|---|---|
| **Propagation channel, interference context, Doppler, propagation delay** | Physical layer | Synchronization, initial access, random access, data channels, channel estimations, low PAPR modulations, link establishment/maintenance due |
| **Propagation delay, beam pattern (very large cells)** | Layer 2 and above | Protocols timing relationship, Inter Radio Access Technology hand-over (Satellite/Cellular) |
| **Non terrestrial networks at access and/or transport level** | Services | 5G services/operational requirements |
| **Propagation delay, beam pattern (very large cells), Cross border coverage (anchor point mobility)** | System architecture | Policy & QoS management, Mobility management, Session management, Traffic steering, multi home transport, eMBMS, Charging policy |

## 3.4 Link budget analysis

### 3.4.1 General link budgets conditions

Following hypotheses have been made concerning the air interface and service requirements.

Concerning the Air Interface, it is derived from NB IOT future standard.

- On downlink use of a PRB of 12 carriers of 15 kHz
- On uplink use of a single tone of 3, 75 kHz or 15 kHz
    - 3,75 kHz chosen for link budgets closure reasons
- BLER of 1% is the target
- Very low C/N values are necessary, for instance (with implementation margins)
    - QPSK 1/3 : -0,5 dB
    - QPSK 1/5 : -2,4 dB
    - QPSK 1/6: -4,6 dB

On the uplink, we consider single tone as equivalent as single carrier for the link budget closure.

For all systems we provide the following conditions and requirements.

- Data rate Requirements
    - Uplink : around 1 kb/s
    - Downlink : around 100 kb/s in 180 kHz
- Propagation Margins
    - We operate in Clear Line Of Sight (CLOS) conditions
    - We assume minimum propagation margins of 5 dB
- Uplink bandwidth
    - 3,75 kHz
- Minimum elevation angle **:**
    - 15 °
- Minimum interference C/I (Carrier to Interference ratio whne same frequency is reused )
    - 10 dB
    - Including C/Im coming from Intermodulation product.

### 3.4.2 Link budget calculation

Not that on Forward Link, we test the two noise figure cases: 9 dB as baseline and 6 dB as improved NF.

#### 3.4.2.1 Case of LEO satellites at 800 km

***Table 3-3 : Forward Link budgets in case LEO 800 km***

| | | | |
|---|---|---|---|
| LEO satellite at 800 km | | | FWD |
| Terminal Type | | | Handheld |
| Noise Figure | (dB) | 9 | 6 |

| Transmission parameters | Unit | | |
|---|---|---|---|
| Used bandwidth this is the case for 1,4 MHz | (khz) | 180 | 180 |
| Down-link Frequency | (GHz) | 2,17000 | 2,17000 |
| Output back off | (dB) | -1,7 | -1,7 |
| Useful EIRP | (dBW) | 28,4 | 28,4 |
| Required EIRP per bloc at saturation | (dBW) | 30,1 | 30,1 |
| Symbol rate | (Ksymb/s) | 161,2 | 161,2 |
| | | | |
| Satellite altitude | km | 800,0 | 800,0 |
| Elevation angle to satellite | ° | 15,0 | 15,0 |
| C/I | (dB) | 10,0 | 10,0 |
| Slant Range | (km) | 2033,0 | 2033,0 |
| Free space propagation | (dB) | -165,3 | -165,3 |
| Atmospheric loss | (dB) | -0,1 | -0,1 |
| Shadowing margins | (dB) | 5,0 | 5,0 |
| | | | |
| Terminal | | | |
| Antenna gain | (dBi) | 0,0 | 0,0 |
| G/T | (dB/K) | -33,6 | -30,6 |
| Polarisation (Circular or Linear) | | L | L |
| Polarisation mismatch loss | (dB) | -3,0 | -3,0 |
| Effective G/T under satellite coverage | (dB/K) | -36,6 | -33,6 |
| (C/No) | (dB Hz) | 52,0 | 53,0 |
| (C/Io ) downlink | (dBHz) | 62,6 | 62,6 |
| C/(No+Io) | (dBHz) | 51,6 | 52,6 |
| Overall C/(No+Io) (including C/Io uplink) (0,5 dB degradation) | (dBHz) | 51,1 | 52,1 |
| Obtained C/N | (dB) | -1,4 | -0,5 |
| Rate | kb/s | 80,5 | 107,4 |
| RX Sensitivity | (dBm) | -113,2 | -114,9 |

***Table 3-4 : Return Link budgets in case LEO 800 km***

| | | |
|---|---|---|
| LEO satellite 800 km Single Tone | | RTN |
| Terminal Type | | Handheld |
| Transmission parameters | Unit | |
| Carrier Bandwidth | (khz) | **3,75** |
| Roll Off | | 0,1 |
| Uplink Frequency | (GHz) | 1,98000 |
| Useful carrier EIRP (under satellite coverage) | (dBm) | 20 |
| | | |
| | | |
| Satellite altitude | km | 800,0 |
| Elevation angle to satellite | ° | 15,0 |
| C/I | (dB) | 10,0 |
| Slant Range | (km) | 2033,0 |
| Free space propagation | (dB) | -164,5 |
| Atmospheric loss | (dB) | -0,1 |
| Shadowing margins | (dB) | 5,0 |
| | | |
| Satellite | | |
| Satelliite G/T | (dB/K) | **-15,25** |
| (C/No) | (dB Hz) | 33,7 |
| (C/Io ) downlink | (dBHz) | 45,3 |
| C/(No+Io) | (dBHz) | 33,4 |
| Overall C/(No+Io) (including 0,5 dB feeder link degradation) | (dBHz) | 32,9 |
| Obtained C/N | (dB) | -2,3990 |
| Rate | kb/s | **1,350** |

#### 3.4.2.2 Case of LEO satellites at 1500 km

***Table 3-5 : Forward Link budgets in case LEO 1500 km***

| | | | |
|---|---|---|---|
| LEO satellite at 1500 km | | | FWD |
| Terminal Type | | | Handheld |
| Noise Figure case | (dB) | 9 | 6 |
| Transmission parameters | Unit | | |
| Used bandwidth this is the case for 1,4 MHz | (khz) | 180 | 180 |
| Down-link Frequency | (GHz) | 2,17 | 2,17 |
| Output back off | (dB) | -1,7 | -1,7 |
| Useful c EIRP | (dBW) | 32,5 | 32,5 |
| Required EIRP per bloc at saturation | (dBW) | 34,2 | 34,2 |
| Symbol rate | (Ksymb/s) | 161,2 | 161,2 |
| | | | |
| Satellite altitude | km | 1500,0 | 1500,0 |
| Elevation angle to satellite | ° | 15,0 | 15,0 |
| C/I (including C/Im) | (dB) | 10,0 | 10,0 |
| Slant Range | (km) | 3259,3 | 3259,3 |
| Free space propagation | (dB) | -169,4 | -169,4 |
| Atmospheric loss | (dB) | -0,1 | -0,1 |
| Shadowing margins | (dB) | 5,0 | 5,0 |
| Terminal | | | |
| Antenna gain | (dBi) | 0,0 | 0,0 |
| G/T | (dB/K) | -33,6 | -30,6 |
| Polarization (Circular or Linear) | | L | L |
| Polarization mismatch loss | (dB) | -3,0 | -3,0 |
| Effective G/T under satellite coverage | (dB/K) | -36,6 | -33,6 |
| (C/No) | (dB Hz) | 50,0 | 53,0 |

| | | | |
|---|---|---|---|
| (C/Io ) downlink | (dBHz) | 60,6 | 62,6 |
| C/(No+Io) | (dBHz) | 49,6 | 52,6 |
| Overall C/(No+Io) (including C/Io uplink0,5 dB degradation) | (dBHz) | 49,1 | 52,1 |
| Obtained C/N | (dB) | -3,4 | -0,5 |
| **Rate** | **kb/s** | 40,3 | 107,4 |
| Rx sensitivity | (dBm) | -116 | -111,9 |

***Table 3-6 : Return Link budgets in case LEO 1500 km***

| LEO satellite at 1500 km | | RTN |
|---|---|---|
| Terminal Type | | Handheld |
| Transmission parameters | Unit | |
| Carrier Bandwidth | (khz) | 3,75 |
| Roll Off | | 0,1 |
| Uplink Frequency | (GHz) | 1,98000 |
| Useful carrier EIRP | (dBm) | 20 |
| | | |
| | | |
| Satellite altitude | km | 1500,0 |
| Elevation angle to satellite | ° | 15,0 |
| C/I | (dB) | 10 |
| Slant Range | (km) | 3259,3 |
| Free space propagation | (dB) | -168,6 |
| Atmospheric loss | (dB) | -0,1 |
| Shadowing margins | (dB) | 5,0 |
| | | |
| Satellite | | |
| G/T | (dB/K) | -13,42 |
| (C/No) | (dB Hz) | 31,4 |
| (C/Io ) downlink | (dBHz) | 45,3 |

| | | |
|---|---|---|
| C/(No+Io) | (dBHz) | 31,2 |
| Overall C/(No+Io) (including C/Io uplink) (0,5 dB degradation) | (dBHz) | 30,7 |
| Obtained C/N | (dB) | -4,5990 |
| **Rate** | **kb/s** | 0,844 |

#### 3.4.2.3 Case of MEO at 10000 km

***Table 3-7 : Forward Link budgets in case MEO 10000 km***

| | | | |
|---|---|---|---|
| MEO satellite 10000 km | | | FWD |
| Terminal Type | | | Handheld |
| Noise Figure | (dB) | 9 | 6 |
| Transmission parameters | Unit | | |
| Used bandwidth this is the case for 1,4 MHz | (khz) | 180 | 180 |
| Down-link Frequency | (GHz) | 2,17000 | 2,17000 |
| Output back off | (dB) | -1,7 | -1,7 |
| Useful carrier EIRP | (dBW) | **44,9** | **44,9** |
| Required EIRP per bloc at saturation | (dBW) | **46,6** | **46,6** |
| Symbol rate | (Ksymb/s) | 161,1 | 161,1 |
| | | | |
| Satellite altitude | km | 10000,0 | 10000,0 |
| Elevation angle to satellite | ° | 15,0 | 15,0 |
| C/I | (dB) | 10,0 | 10,0 |
| Slant Range | (km) | 13524,4 | 13524,4 |
| Free space propagation | (dB) | -181,8 | -181,8 |
| Atmospheric loss | (dB) | -0,1 | -0,1 |
| Shadowing margins | (dB) | 5,0 | 5,0 |
| | | | |
| Terminal | | | |
| Antenna gain | (dBi) | | 0,0 |
| G/T | (dB/K) | -33,6 | -30,6 |

| | | | |
|---|---|---|---|
| Polarization (Circular or Linear) | | L | L |
| Polarization mismatch loss | (dB) | -3,0 | -3,0 |
| Effective G/T under satellite coverage | (dB/K) | -36,6 | -33,6 |
| (C/No) | (dB Hz) | 52,0 | 52,7 |
| (C/Io ) downlink | (dBHz) | 62,6 | 68,6 |
| C/(No+Io) | (dBHz) | 51,6 | 52,6 |
| Overall C/(No+Io) (including C/Io uplink) (0,5 dB degradation) | (dBHz) | 51,1 | 52,1 |
| Obtained C/N | (dB) | -1,4 | -0,5 |
| Rate | kb/s | 80,6 | 107,4 |
| Rx Sensitivity | (dBm) | -113,2 | -114,9 |

***Table 3-8 : Return Link budgets in case MEO 10000 km***

| | | |
|---|---|---|
| MEO satellite Single Tone | | RTN |
| Terminal Type | | Handheld |
| Transmission parameters | Unit | |
| Carrier Bandwidth | (khz) | 3,75 |
| Roll Off | | 0,1 |
| Uplink Frequency | (GHz) | 1,98000 |
| Useful carrier EIRP | (dBWm) | 20 |
| | | |
| | | |
| Satellite altitude | km | 10000,0 |
| Elevation angle to satellite | ° | 15,0 |
| C/I | (dB) | 10,0 |
| Slant Range | (km) | 13524,4 |
| Free space propagation | (dB) | -181,0 |
| Atmospheric loss | (dB) | -0,1 |
| Shadowing margins | (dB) | 5,0 |
| | | |

| | | |
|---|---|---|
| Satellite | | |
| Antenna gain | (dBi) | |
| G/T | (dB/K) | 1,2 |
| (C/No) | (dB Hz) | 33,7 |
| (C/Io ) downlink | (dBHz) | 45,3 |
| C/(No+Io) | (dBHz) | 33,4 |
| Overall C/(No+Io) (including C/Io uplink) (0,5 dB degradation) | (dBHz) | 32,9 |
| Obtained C/N | (dB) | -2,3900 |
| Rate | kb/s | **1,350** |

#### 3.4.2.4 Case of GEO satellite

***Table 3-9 : Forward Link budgets in case GEO***

| | | | |
|---|---|---|---|
| GEO satellite | | | FWD |
| Terminal Type | | | Handheld |
| Noise Figure | (dB) | 9 | 6 |
| Transmission parameters | Unit | | |
| Used bandwidth this is the case for 1,4 MHz | (khz) | 180 | 180 |
| Down-link Frequency | (GHz) | 2,17000 | 2,17000 |
| Output back off | (dB) | -1,7 | -1,7 |
| Useful EIRP | (dBW) | **56,7** | **56,7** |
| Required EIRP per bloc at saturation | (dBW) | **58,4** | **58,4** |
| Symbol rate | (Ksymb/s) | 161,2 | 161,2 |
| | | | |
| Satellite altitude | km | 35786,0 | 35786,0 |
| Elevation angle to satellite | ° | 15,0 | 15,0 |
| C/I | (dB) | 10,0 | 10,0 |
| Slant Range | (km) | 40060,7 | 40060,7 |
| Free space propagation | (dB) | -191,2 | -191,2 |
| Atmospheric loss | (dB) | -0,1 | -0,1 |

| | | | |
|---|---|---|---|
| Shadowing margins | (dB) | 5,0 | 5,0 |
| | | | |
| Terminal | | | |
| Antenna gain | (dBi) | 0,0 | 0,0 |
| G/T | (dB/K) | -33,6 | -30,6 |
| polarization (Circular or Linear) | | L | L |
| polarization mismatch loss | (dB) | -3,0 | -3,0 |
| Effective G/T under satellite coverage | (dB/K) | -36,6 | -33,6 |
| (C/No) | (dB Hz) | 52,0 | 53,0 |
| (C/Io ) downlink | (dBHz) | 62,6 | 62,6 |
| C/(No+Io) | (dBHz) | 51,6 | 52,6 |
| Overall C/(No+Io) (including C/Io uplink0,5 dB degradation) | (dBHz) | 51,1 | 52,1 |
| Obtained C/N | (dB) | -1,4 | -0,5 |
| Rate | kb/s | 80,6 | 107,4 |
| Rx sensitivity | (dBm) | -113,2 | -114,9 |

***Table 3-10 : Return Link budgets in case GEO***

| | | |
|---|---|---|
| GEO satellite Single Tone | | RTN |
| Terminal Type | | Handheld |
| Transmission parameters | Unit | |
| Carrier Bandwidth | (kHz) | 3,75 |
| Roll Off | | 0,1 |
| Uplink Frequency | (GHz) | 1,98000 |
| Useful carrier EIRP | (dBm) | 20 |
| | | |
| | | |
| Satellite altitude | km | 35786,0 |

| | | |
|---|---|---|
| Elevation angle to satellite | ° | 15,0 |
| C/I | (dB) | 10,0 |
| Slant Range | (km) | 40060,7 |
| Free space propagation | (dB) | -190,4 |
| Atmospheric loss | (dB) | -0,1 |
| Shadowing margins | (dB) | 5,0 |
| | | |
| Satellite | | |
| G/T | (dB/K) | 10,65 |
| (C/No) | (dBHz) | 33,7 |
| (C/Io ) downlink | (dBHz) | 45,3 |
| C/(No+Io) | (dBHz) | 33,4 |
| Overall C/(No+Io) (including C/Io uplink) (0,5 dB degradation) | (dBHz) | 32,9 |
| Obtained C/N | (dB) | -2,3900 |
| Rate | kb/s | **1,350** |

### 3.4.3 Conclusions on Space Segment

The following tables give the minimum requirements for Space Segments at RIEP and G/T levels.

***Table 3-11 : Minimum EIRP @ 40-100 kb/s over 180 kHz***

| Constellation | LEO: 800 km | LEO: 1500 km | MEO: 10000 km | GEO: 35786 km |
|---|---|---|---|---|
| Minimum EIRP per 180 kHZ | 27,8 dBW | 32,6 dBW | 44,9 dBW | 56, 7 dBW |

***Table 3-12 : Minimum G/T @ 1 kb/s over 3,75 kHz***

| Constellation | LEO: 800 km | LEO: 1500 km | MEO: 10000 km | GEO: 35786 km |
|---|---|---|---|---|
| Minimum G/T @ 1 kbps | -15,25dB/K | -13,42 dB/K | 1,21 dB/K | 10,65 dB/K |

## 3.5 RRM principles

In order to minimize the signalling overhead, the proposed solution is to simplify as much as possible the protocol exchanges and keep mainly data transmission and in band signalling especially over the return link. The RRM is then kept simple and random access is preferred even to send data when the service is compatible with this access mode. IoT services shall be compatible with this access technique. We consider then that a full frequency reuse is done for every beam and all satellites (if a constellation is considered) and that advanced random access techniques will help to recover from potential collisions.

Taking these assumptions into account, this section provides an evaluation of the number of users that can be served by $km^2$ on the satellite and HAPS systems considered. The table below summarizes the assumptions taken to provide this capacity estimation. As the return link is assumed to be the most dimensioning for IoT and M2M communications, the capacity over return link will be computed.

***Table 3-13: Assumptions for capacity computation***

| System bandwidth | Block size/user bandwidth | Bit rate | Message size | Average message rate | Efficiency of channel usage |
|---|---|---|---|---|---|
| 30MHz | 200kHz/3.75kHz | 1.35 kbps | 200 bits | 1h to 24h | 2 |

We assume that the efficiency of channel usage that can be reached is 2, thanks to repetition and interference cancellation techniques.

The table below summarizes the capacity computation (i.e. the number of users than can be served for a square kilometer) for all satellite and HAPS systems considered.

***Table 3-14: Capacity computation for HAPS and satellite systems***

| | Number of users/km² that can be served (1 hour average) | Number of users/km² that can be served (1 day average) |
|---|---|---|
| HAPS | 72576 | 1741824 |
| LEO | 2420 | 58080 |
| MEO | 1815 | 43545 |
| GEO | 907 | 21772 |

HAPS provides a very high capacity in terms of number of served users and can thus be useful when hot points need to be covered, backed up or extended in terms of capacity.

However it has to be mitigated by the fact that a global coverage is not considered here. If a higher number of HAPS is considered, the interference would increase reducing the possible frequency reuse and thus the number of served users per km².
LEO constellations naturally provide a global coverage and a high capacity regarding the number of served users per $km^2$. In comparison GEO can offer half the capacity of a LEO. This system might be useful to extend coverage of terrestrial networks or to complement the terrestrial systems in dense areas.

## 3.6 Software Reconfiguration as an Enabler for Device Evolution

In this section, we investigate the possible inclusion of Software Reconfiguration solutions for providing added value to Satellite Communication enabled Mobile Devices. In particular, we expect that Software Reconfigurability will be a key feature for equipment which will remain in the market for a substantially longer time compared to today's Smartphones and similar mass market devices. A typical example is the Automotive Communications Use Case, in which equipment remains in the market for the lifetime of a car which can be 10 years and beyond. For such cases, Software Reconfigurability will be a key enable to enable, for example, the addition of new features over its lifetime (corresponding to standardization updates, etc.), to address security issues (e.g., breach of security mechanisms), etc.

For the application of mass-market Software Reconfiguration, we need a framework which meets in particular the following requirements:

1. End-to-End Reconfiguration framework including code development, certification, delivery, installation and execution on the target platform,
2. Security solutions for secure delivery and installation of SW components on the target platform,
3. Certification framework, ensuring seamless certification even after change of (low level) components which are affecting the essential requirements of the European Equipment Directive and thus require a re-certification of the target platform.
4. High level of code efficiency (in terms of power consumption, etc.) and portability to different target platforms.

We have identified the ETSI SW Reconfiguration framework [39] [40] [41] [42] [43] [44] [45] [46] [47 ] as the suitable basis for further investigations. The ETSI solution indeed meets all of the upper requirements. Compared to other available alternative solutions, such as the JTRS Software Communications Architecture (SCA) [49] [50], the ETSI solution has been specifically designed for the needs of mass market commercial equipment and in accordance to Radio Equipment Directive (RED) Articles 3(3)(i) and 4 which introduce Software Reconfigurability in Europe.

Building on the ETSI architecture components on top of the LTE C-V2X Vehicular Communications Solution, we propose the following communications stack in order to address Software Reconfigurability for in-vehicle equipment that supports terrestrial as well as satellite communication [51]:

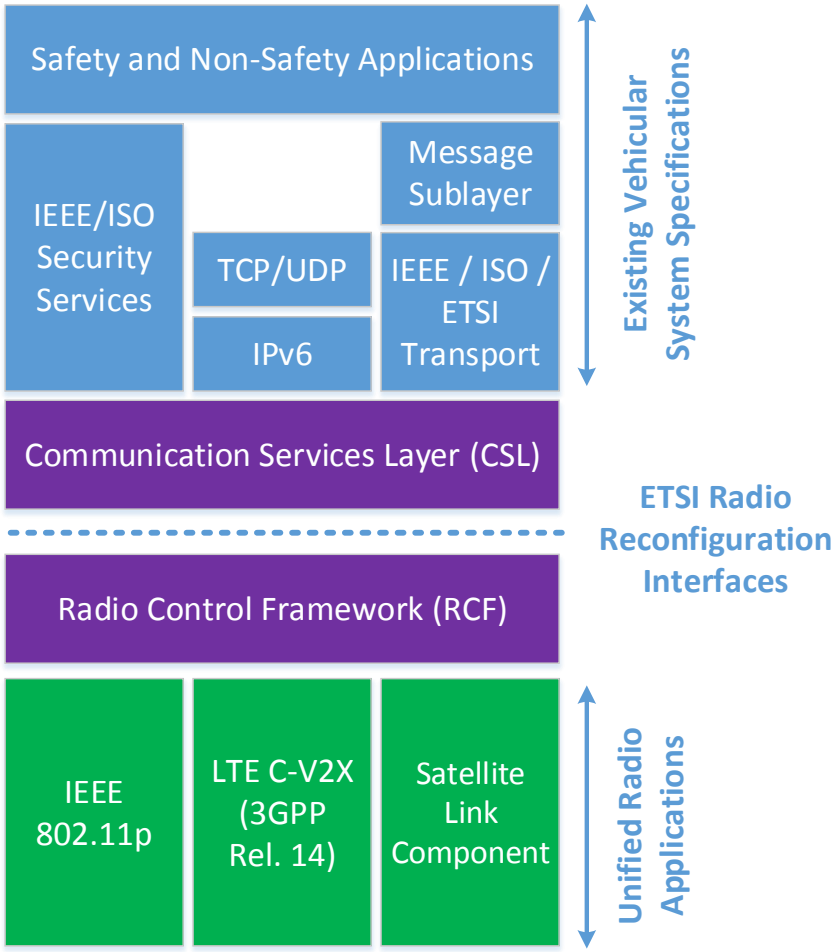


***Figure 3-12: Architecture integrating 3GPP LTE V2X and the ETSI Software Reconfiguration framework.***

The fundamental architecture of a RRS is defined in [40] and consists of Unified Radio Application (URA), Communication Services Layer (CSL), Radio Control Framework (RCF) and Radio Platform (RP) as illustrated in Figure 3-12. This framework enables the provision and usage of (3rd party) software components in a standardized way. A target Radio Application, i.e. a software code altering part of an existing RAT or implementing an additional air interface, e.g., Satellite Link components, CDMA, HSPA, LTE, WiFi, etc., can be downloaded from a RadioApps Store to the target RRS in a form of Radio Application Package (RAP). Since all radio applications exhibit a common behavior from RRS's perspective, those radio applications are called URAs once they are downloaded into the target RRS.

The CSL together with the Multiradio Interface (MURI) are the key components for providing a minimum set of reconfiguration capabilities. The CSL is a layer related to communication

services supporting both generic (e.g., Internet access, etc.) and specific Multi-Radio applications. As shown in Figure 3-13, there are four entities included in the CSL:

- **Administrator**: requests (un)installation of URA, and creates or deletes instances of URA. This typically includes the provision of information about the spectral and computational requirements for each URA, status of each URA, etc. Furthermore, the Administrator includes an Administrator Security Function ensuring confidentiality, integrity, and authenticity of DoC(s) and RAP(s), and the non-repudiation strategy;
- **Mobility Policy Manager**: monitors the radio environments and MD capabilities, requests (de)activation of URA, and provides information about the URA list. It also makes a selection among different RATs and discovers a peer communication equipment and arrangement of associations;
- **Networking stack**: sends and receives user data;
- **Monitor**: presents context information such as Received Signal Strength Indication, Packet Error Rate, Precoding Matrix Indicator, etc. to user upon user's request and transfers context information from URA to proper destination entity.

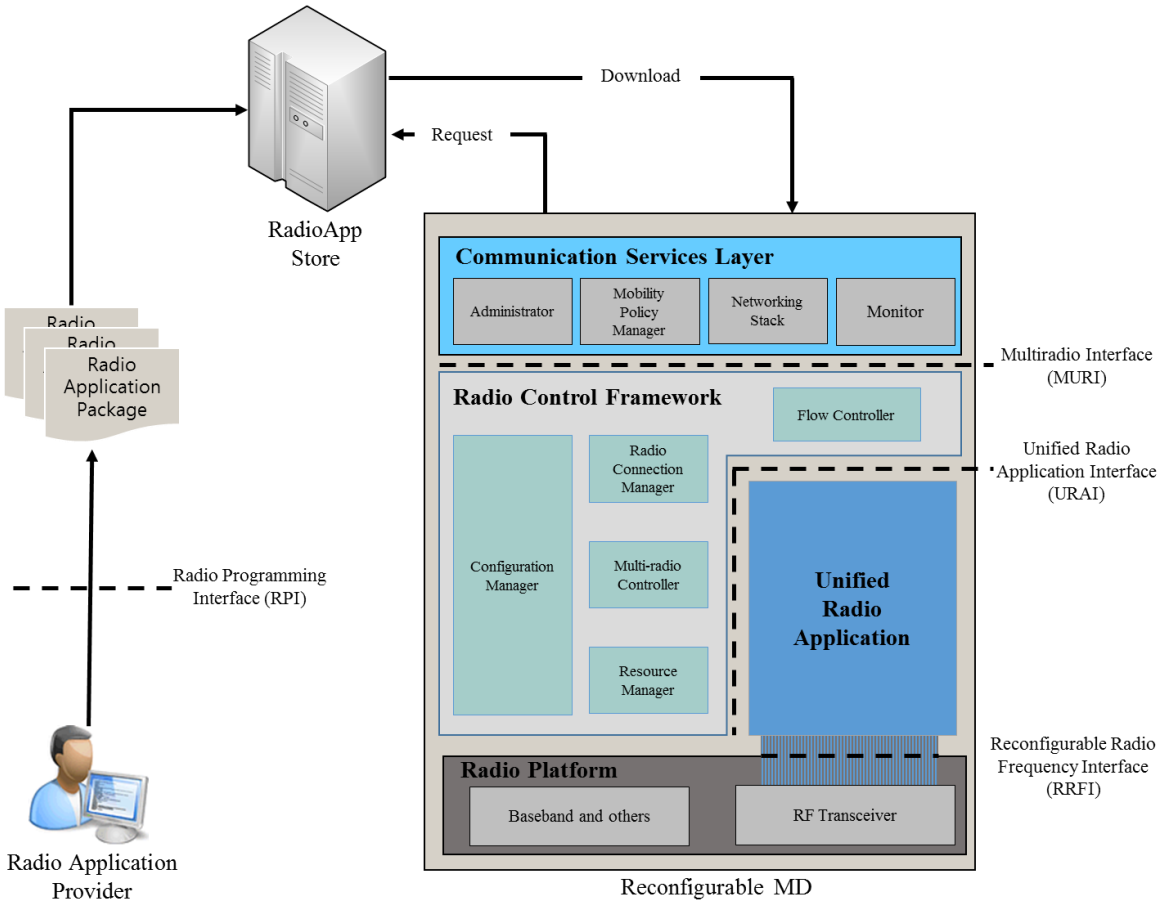


***Figure 3-13: Reconfigurable Radio System Architecture Components 0.***

The above described 4 components, i.e., URA, CSL, RCF and RP, are interconnected through interfaces as follows:

- **MUlti-Radio Interface (MURI)** for interconnecting Communication Services Layer and Radio Control Framework;
- **Unified Radio Application Interface (URAI)** for interconnecting URA and Radio Control Framework;
- **Reconfigurable Radio Frequency Interface (RRFI)** for interconnecting URA and RF Transceiver.

Besides the above written 3 interfaces, Radio Programming Interface (RPI) interfaces Radio Application Provider with RRS. A basic implementation of the reconfiguration framework, comprising the Communication Services Layer (CSL) and the Multiradio Interface (MURI) (to be complemented by the minimum set of required functions in the Radio Control Framework) will employ in particular a number of services provided by MURI [41].

We foresee a specific responsibility in the Mobility Policy Manager (MPM) for the discovery of terrestrial and satellite services, the activation of corresponding features in the target Mobile Device platform and the intelligent routing of services to the concerned air interface. The basic principle is illustrated in the flow chart diagram below:

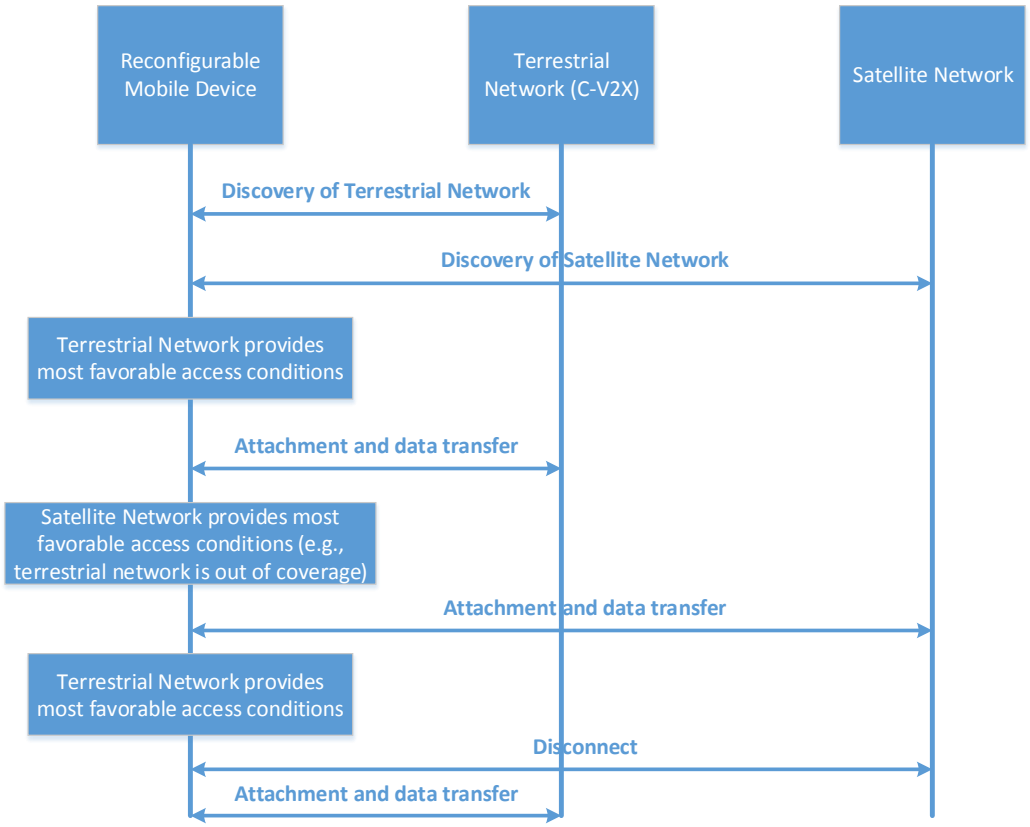


***Figure 3-14: Intelligent Selection of Terrestrial and/or Satellite network.***

Software Reconfigurability is in particular exploited for the following cases:

- In case that a target terrestrial/satellite network (operator) has specific new services to offer (e.g., Device-to-Device communication, etc.), those may be added via Software Update when needed.
- In case that related standards bodies define new essential features, those can be added a-posteriori through software updates.
- In case that a short-term emergency occurs, e.g. a security breach of the encryption chain, corresponding new and updated features can be provided through software upgrades.

With the features introduced above, corresponding Communication Components will have the capability to remain relevant over a lifetime of 10 years and beyond. Vehicular applications are a suitable use cases, but also other applications of substantial lifetime are suitable target applications.

# 4 5G emulation platform

## 4.1 Test bed specifications

The testbed emulates a point-to-point communication between the transmitter and the terminal. The transmitter can either be located in the gateway (bend-pipe satellite) or in the satellite (regenerative satellite). Both uplink and downlink transmissions are considered.

The main intend of the test bed is to assess the difference between the theoretical performance, relying on channel capacity as described in 2.4.3, and real-world performance, including

- Phase noise from the terminal, but also from the satellite in case of bend-pipe satellites
- Synchronization imperfections, especially for downlink transmissions
- Propagation channel

In addition to assess the impact of phase noise and of the propagation channel, this will allow to define the required time and frequency synchronization accuracy, which directly impact the receiver complexity.

## 4.2 Test bed proposed architecture

The 5G radio interface proof of concept for NB-IoT satellite use case is based on CEA's proprietary flexible and programmable platform and CEA channel emulator. A flexible implementation of the IoT radio interface will be investigated with special care on link level performance evaluation.

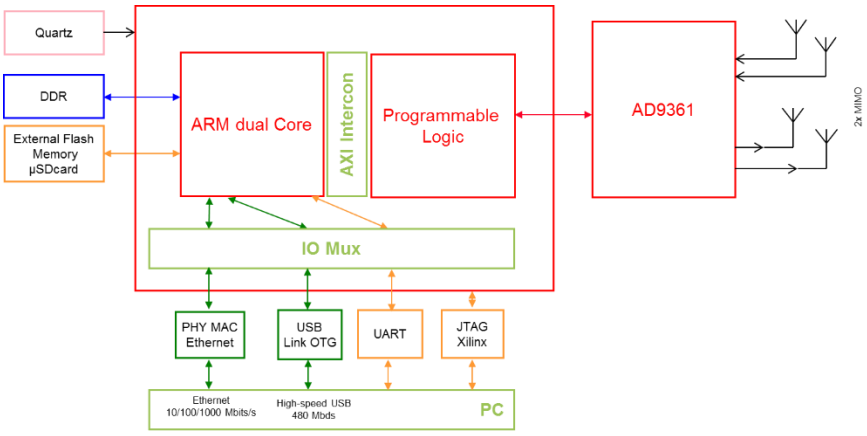


***Figure 4-1: Overview of CEA platform.***

The hardware platform is based on a hybrid FPGA integrating programmable logic and an ARM processor, ADC, DAC, and various interfaces. The combination of the FPGA and the

ARM processor allows the easy deployment of embedded Linux and is well suited for software-defined radio implementation and rapid prototyping.

Ethernet PHY/MAC (IPv6 compatible) is provided for easy LAN connectivity. A brief architecture description is depicted in Figure 4-1. A specific daughterboard is being developed to address the satellite L-band using AD9361 module. AD9361 RF front end is a software tunable component across a wide frequency range (70 MHz to 6.0 GHz) with a channel bandwidth from 200 kHz up to 56 MHz.

Experiments will be carried out to quantify performance through the CEA channel emulator. The CEA channel emulator has the following characteristics:

- Frequency range 200MHz – 6GHz
- Bandwidth up to 125MHz
- Noise and inference modelling
- Mobility modelling (Doppler)

The channel emulator will be used to evaluate the radio interface through the emulation of specific models developed in the context of the project.

The test bed depicted in Figure 4-2 will be used to evaluate the radio interface. The evaluation of advanced features using external processing elements (PC) will be considered (hardware-in-the-loop approach). Dedicated software tools are developed to visualize selected KPIs (such as BER, SNR, PAPR, spectral signal properties).

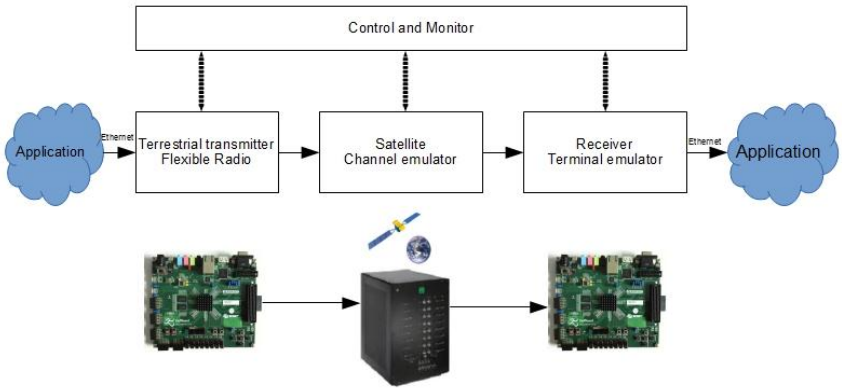


***Figure 4-2: Proposed testbed for satellite performance assessment.***

As an example, we depict in Figure 4-3 a screenshot of the Graphical user Interface developed to monitor KPIs and to control the HW platform. The PHY layer integrates synchronization and channel estimation scheme using a dedicated frame format. The transmitted signal is acquired by the RF chain and the baseband processing, including synchronization (time and frequency), channel estimation is then proceed. Figure of merits of the proposed PHY is under investigation using the channel emulation platform fed by the project channel model.

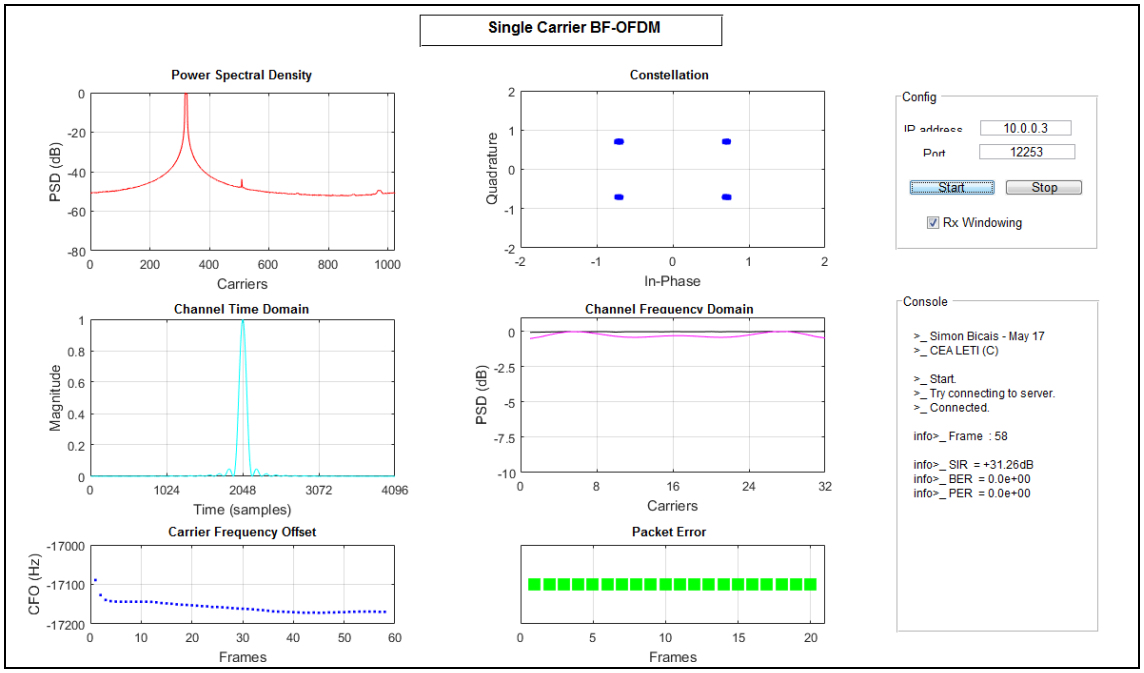


***Figure 4-3: Screenshot of the Graphical User Interface developed for the project monitoring performance of NB IoT using SC-FDMA on top of BF OFDM waveform.***

## 4.3 Test cases definition

### 4.3.1 Waveforms performance assessment in ideal conditions

It is first proposed to assess the performance of the different waveforms in ideal conditions, i.e. without taking into account terminal impairments (synchronization issues, phase noise, non-linearities at UL) and satellite impairments (Doppler shift, phase noise, non-linearities).

NB-IoT modulations, i.e. OFDM and SC-FDMA, will be compared to FSK-modulation on top of OFDM in terms of envelope fluctuations (IAPR) and of capacity in an AWGN channel. The low and high data rate channels will be both considered, as done in Section 3.1.1.3.

### 4.3.2 Performance assessment with realistic channel coefficients

A realistic channel model will then be considered. The received power fluctuates due to time-changing interference, which is alternatively constructive and destructive.

### 4.3.3 Performance degradation due to terminal impairments

It is proposed to assess the degradation due to terminal impairments for the case of low and high data rate channels. More specifically, phase noise and synchronization errors at the terminal will be assessed in terms of capacity loss compared to the ideal case. The downlink will be here considered since synchronization issues are considered.

### 4.3.4 Performance degradation due to satellite impairments

Finally, performance on uplink and downlink will be assessed considering satellite impairments, mainly including Doppler shift.

# 5 Conclusion

In this document, seamless operation of 5G UE via a satellite communication component has been investigated. Low data rates communications have been targeted for IoT and voice services and the satellite component is mainly used for coverage extension or as back-up service. Forecast waveforms for IoT services in future 5G systems have been analyzed and compared. A new modulation scheme, called turbo-FSK on top of BFDM, has also been proposed for performance improvements with reduced peak-to-average power ratio.

Link budget have been performed to demonstrate the feasibility of 5G UE operation via satellite. The required performance for the satellite platform is in line with current state-of-the-art technology. Depending on the considered platform (satellite/HAPS), tens of thousands to a few millions of users can be served by the non-terrestrial component

The document also describes the necessary modifications to operate on 5G systems in order to take satellite and HAPS specifics into account. Emphasis has mainly been put on RRM principles and mass-market software reconfiguration for device evolution with very large lifetime (above 10 years).

This document finally specifies a test bed to demonstrate the 5G interface performance via selected space segment configurations under representative interference/mobility conditions.

# 6 ANNEXES

## 6.1 ANNEX 1: Channel capacity definition

The classical expression of the capacity $C$ is given by

$$C = Blog_2(1 + SNR)$$

where $C$ is expressed in bits/s/Hz. Any technique of transmission is bounded by the capacity, and getting close to it has been the purpose of countless researches. Reaching the limit would signify that the resource in bandwidth, time and rate is used in the most efficient way possible. In that way, having a system close the capacity would be a huge benefit in our context.

In order to express the limit using the quantities defined previously, we define $\eta_{\max} \frac{C}{B}$ as the maximum achievable spectral efficiency. Using the SNR definition, the limit can now be expressed

which thus gives the maximum energy efficiency possible for a given spectral efficiency, for an arbitrarily small level of error.

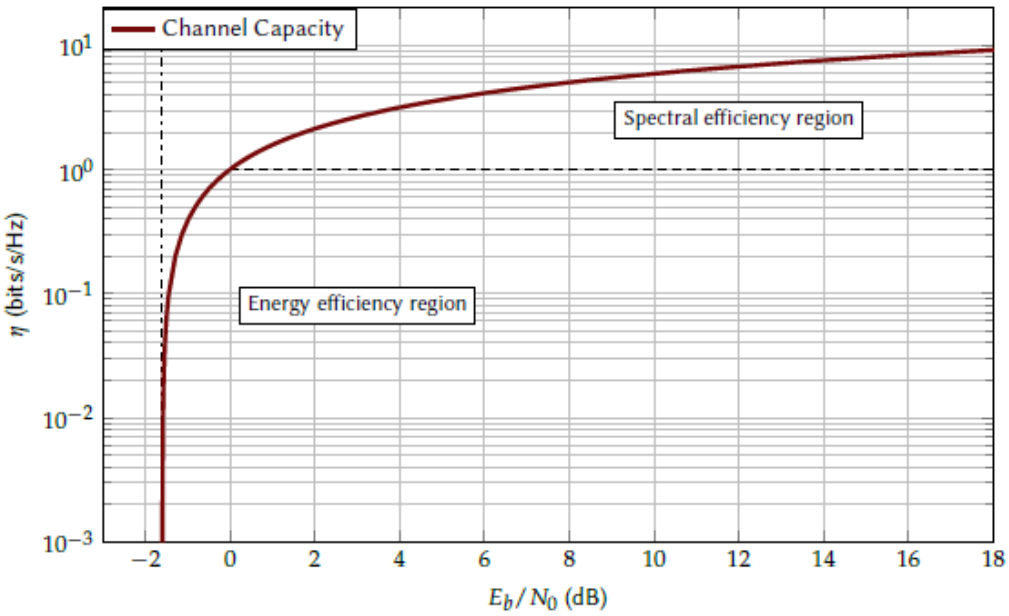


***Figure 6-1: Theoretical spectral efficiency as function of E_b/N_0***

On Figure 6-1, the limit has been represented versus the energy efficiency. The plot is generally divided in two main regions [31]. The first region is the spectral efficiency region. In this area, spectral efficiency is high (>1) while the $\frac{E_b}{N_0}$ is high too: this region

concerns techniques designed for very high data rates without considering energy efficiency as a major constraint.

In the second region, the energy efficiency region, the level of $\frac{E_b}{N_0}$ is low but so is the spectral efficiency: this area concerns techniques where the energy efficiency constraint is very high, while less data rate is required, or more bandwidth usage is accepted.

From the closed form of the limit, the mathematical limit when $\eta$ tends toward 0 can be shown to be $\frac{E_b}{N_0} = \log(2) \approx -1.59\text{dB}$. No technique can function properly at a $\frac{E_b}{N_0}$ lower than this ultimate value.

# References

[1] F. P. Fontan, M. Vazquez-Castro, C. E. Cabado, J. P. Garcia and E. Kubista, "Statistical modeling of the LMS channel," in IEEE Transactions on Vehicular Technology, vol. 50, no. 6, pp. 1549-1567, Nov 2001.

[2] Chun Loo, "A statistical model for a land mobile satellite link," in IEEE Transactions on Vehicular Technology, vol. 34, no. 3, pp. 122-127, Aug. 1985.

[3] H. Smith, S. K. Barton, J. G. Gardiner, and M. Sforza, “Characterization of the land mobile-satellite (LMS) channel at L and S bands: Narrowband measurements”, Bradford, ESA AOPs 104 433/114 473, 1992.

[4] A. Jahn and E. Lutz, “Propagation Data and channel model for LMS systems”, Final Rep. ESA PO 141 742. DLR, 1995.

[5] F. Murr, S. Kastner-Puschl, B. Bolzano, and E. Kubista, “Land Mobile Satellite narrowband propagation measurement campaign at Ka-Band”, ESTEC Contract 9949/92/NL, Final Rep., 1995.

[6] Prieto-Cerdeira, R., Perez-Fontan, F., Burzigotti, P., Bolea-Alamañac, A. and Sanchez-Lago, I., “Versatile two-state land mobile satellite channel model with first application to DVB-SH analysis”, Int. J. Satell. Commun. Network., 28: 291–315., June 2010.

[7] ITU-R P.681-9, “Propagation data required for the design of earth-space land mobile telecommunication systems”, Sept. 2016.

[8] 4G LTE World Coverage Map." http://www.worldtimezone.com/4g.html”. Accessed: January 24, 2017.

[9] 5G white paper." NGMN 5G Initiative”, Feb 2015.

[10] T. Rebbeck, M. Mackenzie, and N. Afonso,” Low-powered wireless solutions have the potential to increase the M2M market by over 3 billion connections." Analysys Mason, Sept 2014.

[11] D. Evans, “The internet of things - how the next evolution of the internet is changing everything." Cisco White Paper, April 2011.

[12] Machina Research, “Lpwa technologies - unlock new iot market potential." A White Paper prepared for the LoRa Alliance, Sept 2014.

[13] “Low throughput networks (ltn): Protocol and interfaces." ETSI Group Speci_cation GS LTN 003, V1.1.1, Sept 2014.

[14] A. Augustin, J. Yi, T. Clausen, and W. M. Townsley, “A study of lora: Long range & low power networks for the internet of things," Sensors, vol. 16, no. 9, p. 1466, 2016.

[15] SigFox website." http://www.sigfox.com/.” Accessed: January 24, 2017.

[16] LoRa Alliance." https://www.lora-alliance.org/." Accessed: January 24, 2017.

[17] O. Seller and N. Sornin, "Low power long range transmitter," Aug 2014.

[18] A. Springer, W. Gugler, M. Huemer, L. Reindl, C. C. W. Ruppel, and R. Weigel, "Spread spectrum communications using chirp signals," in IEEE/AFCEA EUROCOMM 2000. Information Systems for Enhanced Public Safety and Security (Cat. No.00EX405), pp. 166-170, 2000.

[19] D. Chu, "Polyphase codes with good periodic correlation properties (corresp.)," IEEE Transactions on Information Theory, vol. 18, pp. 531-532, Jul 1972.

[20] "Lora modulation theory." Semtech Technical Brief, Jan.

[21] "802.15.4k: Low-Rate Wireless Personal Area Networks (LR-WPANs) Amendment 5: Physical Layer Specifications for Low Energy, Critical Infrastructure Monitoring Networks.." IEEE Standard for Local and metropolitan area networks, Aug 2013.

[22]X. Xiong, K. Zheng, R. Xu, W. Xiang, and P. Chatzimisios, "Low Power Wide Area Machine-to-Machine Networks: Key Techniques and Prototype," IEEE Communications Magazine, vol. 53, pp. 64-71, September 2015.

[23] "How rpma works." A White Paper by Ingenu. Retrieved from the Ingenu website.

[24] T. Myers, "Random phase multiple access system with meshing," Aug 2010.

[25] "LTE Evolved Universal Terrestrial Radio Access (E-UTRA): Physical Channels and Modulation." 3GPP TS 36.211, V13.2.0, Release 13, Aug 2016.

[26] "Whitepaper narrowband internet of things." Rohde & Schwarz, Aug 2016.

[27] "LTE Evolved Universal Terrestrial Radio Access (E-UTRA): Multiplexing and Channel Coding." 3GPP TS 36.212, V12.6.0, Release 12, Oct 2015.

[28] R. Ratasuk, B. Vejlgaard, N. Mangalvedhe, and A. Ghosh, "Nb-iot system for m2m communication," in 2016 IEEE Wireless Communications and Networking Conference, pp. 1-5, April 2016.

[29] Y.-P. E. Wang, X. Lin, A. Adhikary, A. Gr□bvlen, Y. Sui, Y. W. Blankenship, J. Bergman, and H. S. Razaghi, "A primer on 3gpp narrowband internet of things (nb-iot)," CoRR, vol. abs/1606.04171, 2016.

[30] H. G. Myung, J. Lim, and D. J. Goodman, "Single carrier fdma for uplink wireless transmission," IEEE Vehicular Technology Magazine, vol. 1, pp. 30-38, Sept 2006.

[31] J. Proakis, Digital Communications 3rd Edition. Communications and signal processing, McGraw-Hill, 1995.

[32] Y.Roth, J.-B. Dore, L. Ros, and V. Berg, Turbo-FSK: A New Uplink Scheme for Low Power Wide Area Networks," in {2015 IEEE 16th International Workshop on Signal Processing Advances in Wireless Communications (SPAWC), June 2015, pp. 81--85.J.

[33] Demmer, R. Gerzaguet, J-B. Doré, D. Le Ruyet, Dimitri Kténas. « Block-Filtered OFDM: a novel waveform for future wireless technologies », ICC2017, Wireless Communications Symposium, Paris, France, May 2017.

[34] Y. Roth, J.-B. Dor´e, L. Ros, and V. Berg, “Turbo-FSK: A New Uplink Scheme for Low Power Wide Area Networks,” in 2015 IEEE 16th International Workshop on Signal Processing Advances in Wireless Communications (SPAWC), Stockholm, Sweden, June 2015, pp. 81–85.

[35] ——, A Comparison of Physical Layers for Low Power Wide Area Networks. Springer International Publishing, 2016.

[36] D. Chu, “Polyphase codes with good periodic correlation properties (corresp.),” IEEE Transactions on Information Theory, vol. 18, no. 4, pp. 531–532, July 1972.

[37] S. Zhou, H. Chen, Y. Xiong, and L. Gu, “The study on the algorithm of frequency offset estimation in broadband wireless access systems,” in 2007 IET Conference on Wireless, Mobile and Sensor Networks (CCWMSN07), Dec 2007, pp. 750–754.

[38] V. Mannoni, V. Berg, F. Dehmas, and D. Noguet, “A Flexible Physical Layer for LPWA Applications,” CROWNCOM, 2017.

[39] ETSI EN 302 969 V1.2.1 (2014-11), Reconfigurable Radio Systems (RRS); Radio Reconfiguration related Requirements for Mobile Devices

[40] ETSI EN 303 095 V1.2.1 (2015-06), Reconfigurable Radio Systems (RRS); Radio Reconfiguration related Architecture for Mobile Devices

[41] ETSI EN 303 146-1 V1.2.1 (2015-11), Reconfigurable Radio Systems (RRS); Mobile Device Information Models and Protocols; Part 1: Multiradio Interface (MURI)

[42] ETSI EN 303 146-2 V1.2.1 (2016-06), Reconfigurable Radio Systems (RRS); Mobile Device (MD) information models and protocols; Part 2: Reconfigurable Radio Frequency Interface (RRFI)

[43] ETSI EN 303 146-3 V1.2.1 (2016-08), Reconfigurable Radio Systems (RRS); Mobile Device (MD) information models and protocols; Part 3: Unified Radio Application Interface (URAI)

[44] ETSI EN 303 146-4 V1.2.1 (2017-04),, Reconfigurable Radio Systems (RRS); Mobile Device (MD) information models and protocols; Part 4: Radio Programming Interface (RPI)

[45] ETSI TR 103 087 V1.1.1 (2016-06); Reconfigurable Radio Systems (RRS); Security related use cases and threats in Reconfigurable Radio Systems

[46] ETSI TS 103 436 V1.1.1 (2016-08); Reconfigurable Radio Systems (RRS); Security requirements for reconfigurable radios

[47] ETSI TR, under development, Reconfigurable Radio Systems (RRS); Applicability of RRS with existing Radio Access Technologies and core networks Security aspects

[48] DIRECTIVE 2014/53/EU OF THE EUROPEAN PARLIAMENT AND OF THE COUNCIL of 16 April 2014 on the harmonization of the laws of the Member States relating to the making available on the market of radio equipment and repealing Directive 1999/5/EC, http://eur-lex.europa.eu/legal-content/EN/TXT/?uri=celex:32014L0053

[49] SOFTWARE COMMUNICATIONS ARCHITECTURE SPECIFICATION, Joint Tactical Networking Center (JTNC), August 2015, V4.1, available at http://www.public.navy.mil/jtnc/sca/Pages/default.aspx

[50] SOFTWARE COMMUNICATIONS ARCHITECTURE SPECIFICATION USER'S GUIDE, Version: 4.1, 23 February 2016 , available at http://www.public.navy.mil/jtnc/sca/Pages/default.as

[51] Evolution of DSRC to LTE V2X enabled through Software Reconfiguration; Markus Mueck, Seungwon Choi, Taesang Choi, Emilio Calvanese Strinati, Yong Jin, Kyunghoon Kim, Heungseop Ahn, Vladimir Ivanov, Thomas Haustein, Valerio Frascolla, Scott Cadzow, Francois Ambrosini; submitted to IEEE Communications Magazine